

Quasi-Parton Distribution Function in Lattice Perturbation Theory

Xiaonu Xiong^{*},¹ Thomas Luu[†],^{1,2} and Ulf-G. Meißner^{‡3,1,2}

¹*Institute for Advanced Simulation,
Institut für Kernphysik and Jülich Center for Hadronphysics,
Forschungszentrum Jülich, D-52428 Jülich, Germany*

²*JARA -High Performance Computing,
Forschungszentrum Jülich, D-52428 Jülich, Germany*

³*Helmholtz-Institut für Strahlen- und Kernphysik and Bethe Center for Theoretical Physics,
Universität Bonn, D-53115 Bonn, Germany*

(Dated: August 3, 2018)

Abstract

Large momentum effective field theory provides a new direction for lattice QCD calculations of hadronic structure functions, such as parton distribution functions (PDFs), meson distribution amplitudes, and so on, directly with x -dependence. In the framework of Lattice Perturbation Theory (LPT), we compute the one-loop quark-in-quark quasi-PDF with the naïve fermion action (\tilde{q}^{nv}) and quasi-PDF with Wilson-Clover action (\tilde{q}^{WC}) and show that \tilde{q}^{nv} reduces to the continuum quasi-PDF in the continuum limit. We point out, however, that the continuum limit and massless quark limit do not commute. We find that the condition to recover the same collinear divergence that the quasi-PDF has in continuum QCD is $aP_3^2 \approx m$ and $m \ll P_3$, while the condition to fully recover the continuum quasi-PDF is $aP_3^2 \ll m \ll P_3$, where P_3 is the momentum in the direction of the quark's motion (longitudinal direction). These two conditions are based on perturbation calculations and should not be applied to non-perturbative calculations because the non-perturbative effects cure the collinear divergence. The correction to the quasi-PDF using the naïve fermion action is due to the Wilson term and can be viewed as an $\mathcal{O}(a^1)$ correction. For nonzero r , the $\mathcal{O}(a^1)$ corrections are subsequently mixed with the quasi-PDF using the naïve fermion action.

PACS numbers: *11.15.Ha, 12.38.Bx, 12.38.Gc*

^{*} x.xiong@fz-juelich.de

[†] t.luu@fz-juelich.de

[‡] meissner@hiskp.uni-bonn.de

I. INTRODUCTION

The parton distribution functions (PDFs) provide essential information for understanding various aspects of the internal structure of hadrons, such as the nucleon spin structure [1–3] and the flavor structure of the proton [4, 5]. Thanks to the concept of factorization, which separates the perturbatively calculable short-range processes and the complex long-range behavior, the latter one is absorbed into PDFs [6]. PDFs also can be widely used as important inputs for high-energy experiments involving hadrons that, for example, probe new physics at hadron colliders [7, 8]. The experimental determination and application of PDFs are based on their universality, which allows one to extract the PDFs from various types of high-energy scattering processes measured in different types of experiments. The factorization and universality of the PDFs play a central role in QCD predictions. Therefore, the determination of PDFs has been a long-standing key task in QCD. Although PDFs can be measured experimentally, there are still some regions that experiments can not cover or present large uncertainties (e.g. PDFs at small and large Bjorken x and gluon PDFs) [9, 10]. Theoretical studies can help provide more precise and complete PDFs. Due to the non-perturbative nature of hadrons, the theoretical study of their internal structure requires non-perturbative methods. Previous studies of hadronic PDFs used QCD models and Ads/CFT QCD. However, the model dependence in those studies has limited their predictive power. Lattice QCD provides so far the only reliable first-principle non-perturbative QCD method, but calculating PDFs through lattice QCD has its intrinsic difficulties.

The light-cone quark PDFs are defined via [11]

$$q_{\Gamma}(x) = \int \frac{d\xi^-}{4\pi} e^{-ixP^+\xi^-} \left\langle P \left| \bar{\psi}(\xi^-) \Gamma \mathcal{P} \left\{ \exp \left[-ig \int_0^{\xi^-} d\eta^- A^+(\eta^-) \right] \right\} \psi(0) \right| P \right\rangle, \quad (1)$$

where $\Gamma = \gamma^+, \gamma^+\gamma_5, \gamma^+\gamma^\perp$ and the light-cone components of a vector v^μ are $v^\pm = (v^0 \pm v^z)/\sqrt{2}$, $v^\perp = v^{1,2}$. The different γ -matrices correspond to the unpolarized PDF, helicity distribution function and transversity distribution function, respectively. The path-ordered exponential is the gauge link, which ensures the gauge invariance of the non-local quark correlator. The light-cone PDFs are based on light-cone correlation functions while lattice QCD correlators are evaluated in Euclidean space-time. The field separation ξ^- becomes complex in Euclidean space-time. Consequently, lattice QCD can not calculate the explicit x -dependence of any PDF directly. Instead, lattice QCD calculations focus on the PDF's Mellin moments which reduce to local operator matrix elements

$$q^n = \int_0^1 dx x^{n-1} q(x) \sim \left\langle P \left| \bar{\psi}(0) \gamma^{\{+} \overleftrightarrow{D}^+ \dots \overleftrightarrow{D}^{+\} \psi(0) \right| P \right\rangle - \text{trace}. \quad (2)$$

These can be calculated directly on the lattice. The PDFs are then reconstructed from these Mellin moments. However, due to operator mixing and discretization errors, the high moments are very difficult to calculate.

The proposed large momentum effective field theory provides the ability to calculate PDFs with their x -dependence directly on the lattice. In the large momentum effective field theory, the light-cone PDFs are accessible from particular pure spatial correlation functions: the so-called quasi-PDFs, which are defined as [12, 13]

$$\tilde{q}_{\Gamma}(x, \mu^2, P^z) = \int \frac{dz}{4\pi} e^{ixP^z z} \left\langle P \left| \bar{\psi}(z) \tilde{\Gamma} \mathcal{P} \left\{ \exp \left[-ig \int_0^z dz' A^z(z') \right] \right\} \psi(0) \right| P \right\rangle, \quad (3)$$

where again $\tilde{\Gamma} = \gamma^z, \gamma^z \gamma_5, \gamma^z \gamma^\perp$. The gauge link lies in the z -direction. The fact that the field separation z is purely spatial and no longer complex enables such a quantity to be calculated directly on the lattice. The quasi-PDFs and light-cone PDFs are then related through a matching condition [14]

$$\tilde{q}(x) = \int_{-1}^1 \frac{dy}{|y|} Z\left(\frac{x}{y}\right) q(y) + \mathcal{O}\left(\frac{M_N^n}{(P^z)^n}\right) + \mathcal{O}\left(\frac{\Lambda_{QCD}^n}{(P^z)^n}\right), \quad (4)$$

where Z is the matching factor and the last two terms refer to the target mass and higher twist corrections, respectively. The proof of the above matching condition can be found in Refs. [15, 16]. The target mass corrections of quark PDFs has been studied in Ref. [17]. The quasi-PDFs are assumed to have the same infrared behavior as the light-cone PDFs, and under this assumption, the matching factor Z is totally controlled by the ultraviolet (UV) behavior of quasi-PDF and light-cone PDF. As a consequence, the matching factor can be calculated by perturbation theory. The matching factor Z is calculated up to $\mathcal{O}(\alpha_s)$ in continuum QCD in Refs. [14, 15] and the renormalization of quasi-PDFs up to $\mathcal{O}(\alpha_s^2)$ is studied in Ref. [18]. The matching scheme in position space is studied in Ref. [19]. Some possible improved definitions of quasi-PDFs are suggested in Refs. [20, 21]. The matching for the PDF's generalizations, Generalized Parton Distributions (GPDs), have been studied in Refs. [22, 23]. Lattice simulations of quasi-unpolarized parton distributions, quark helicity distributions and transversity distributions have been performed in Refs. [17, 24, 25]. LPT calculations of the quasi-PDF using Wilson fermions up to $\mathcal{O}(\alpha_s^1, a^0)$ can be found in Ref. [26]. In this work they discuss the discrepancy of the IR behavior between Euclidean and Minkowski quasi-PDFs. Ref. [27] provides a solution to this discrepancy. Recently, the perturbative and nonperturbative renormalization of quasi-PDFs on the lattice have been studied in Refs. [28, 29] using the RI scheme and lattice simulations of quasi-PDFs with renormalization in the RI/MOM scheme is presented in Ref. [30].

In this work we focus on calculating the one-loop quark-in-quark quasi-PDF (unpolarized) from lattice perturbation theory. We use both the naïve fermion and Wilson-Clover fermion actions as our discretization. We find that, due to lattice artifacts, the collinear divergence is absent in the LPT-calculated quasi-PDF when the lattice spacing is not too small, even after extending the LPT-calculated quasi-PDFs to Minkowski space. Furthermore, since the massless quark limit and the continuum limit do not commute in the LPT-calculated quasi-PDFs, the exchange of these two limits leads to different IR (collinear) behavior of the quasi-PDF in LPT at finite lattice spacing. The correct condition that reproduces the same collinear divergence in the continuum limit quasi-PDF is $aP_3^2 \approx m$ and $m \ll P_3$. The limit for fully reproducing the quasi-PDF in continuum QCD is $aP_3^2 \ll m \ll P_3$. These two conditions should be constrained to perturbative calculations, because the non-perturbative effects in non-perturbative lattice calculations remove the collinear divergence. We also observe that the $\mathcal{O}(a^1)$ corrections turn out to be mixed with the $\mathcal{O}(a^0)$ quasi-PDF. The presence of this mixing limits the lattice perturbation calculation to a ballpark estimation of the matching factor between lattice and continuum. As such, a non-perturbative matching is more appropriate and will be studied in future work.

The rest of the paper is organized as follows: in Sec. II we introduce the Wilson-Clover fermion action and naïve fermion action, as well as their corresponding Feynman rules. In Sec. III we describe the calculation method and present the analytical result of the quasi-PDF in LPT with the naïve fermion action, and show that the quasi-PDF is an integral over

transverse momentum \mathbf{k}_\perp . We also compare the $a \rightarrow 0$ limit of our result and the quasi-PDF directly calculated in continuum QCD and discuss the collinear divergence term in the two quasi-PDFs. We will also shortly present the calculation of quasi-PDF in LPT with Wilson-Clover fermion action. In Sec. IV we present our numerical results for the quasi-PDF in LPT and its comparison with the continuum quasi-PDF. We conclude in Sec. V.

II. NAÏVE AND WILSON-CLOVER FERMION ACTION AND FEYNMAN RULES

The Wilson-Clover action is given by

$$S = -\frac{1}{2} \sum_{x,\mu} [\bar{\psi}(x) (r - \gamma_\mu) U_\mu(x) \psi(x + a\hat{\mu}) + \bar{\psi}(x + \mu) (r + \gamma_\mu) U_\mu^\dagger(x - a\hat{\mu}) \psi(x)] \\ + \sum_x \left[(4r + m) \bar{\psi}(x) \psi(x) - \sum_{\mu,\nu} c_{SW} g_s \frac{a}{4} \bar{\psi}(x) \sigma_{\mu\nu} \hat{F}_{\mu\nu}(x) \psi(x) \right], \quad (5)$$

where the gauge field strength tensor is defined as

$$\hat{F}_{\mu\nu} \equiv \frac{1}{8} (Q_{\mu\nu} - Q_{\nu\mu}), \quad (6)$$

and $Q_{\mu\nu}$ denotes the sum of plaquette loops. We use the plaquette gauge action for gluon. The Wilson-Clover fermion action violates chiral symmetry explicitly through the terms proportional to r . We choose Wilson-Clover fermions because we focus only on the unpolarized parton distribution functions and such terms do not depend crucially on chiral symmetry (and breaking thereof). Further, Wilson-Clover fermions provide a reasonable computational cost for most practical lattice calculations.

The Wilson-Clover fermion's on-shell condition can be solved from the lattice discretized Dirac equation

$$\left[i \sum_\mu \gamma_\mu \widehat{P}_\mu + r \sum_\mu \left(\frac{2}{a} - \widetilde{P}_\mu \right) + 2m \right] U(P) = 0, \quad (7)$$

where the lattice momenta are

$$\widehat{P}_\mu = \frac{2}{a} \sin \frac{aP_\mu}{2}, \quad \widetilde{P}_\mu = \frac{2}{a} \cos \frac{aP_\mu}{2}. \quad (8)$$

The Dirac equation gives the dispersion relation for the Wilson-Clover fermions

$$P_4 = \frac{1}{a} \sinh^{-1} \left(\frac{1}{\sqrt{2}} \left\{ \frac{1}{(1-r^2)^2} \left[2(r^2+1)(am+2r)(a^2r\widehat{P}_3^2+am) \right. \right. \right. \\ \left. \left. \left. - \frac{1}{2}a^2(r^4+2r^2-1)\widehat{P}_3^2 + 4r^2 - (a^2r^2\widehat{P}_3^2+2ram+2r^2) \right. \right. \right. \\ \left. \left. \left. \times \sqrt{a^4(2r^2-1)\widehat{P}_3^4 + 4a^2\widehat{P}_3^2(amr+1) + 4am(am+2r) + 4} \right] \right\}^{\frac{1}{2}} \right), \quad (9)$$

in which we have set the quark moving along the z -direction $P_\mu = (0, 0, P_3, P_4)$ and we keep this momentum setup for the parent quark throughout the paper. In the continuum limit, this reduces to the conventional on-shell condition

$$\lim_{a \rightarrow 0} P_4 = \sqrt{P_3^2 + m^2}. \quad (10)$$

The Feynman rules for Wilson-Clover fermion action can be found in Ref. [31]. The quark propagator is given by

$$S_F(k) = 2 \left[\frac{-i \sum_{\mu} \gamma_{\mu} \widehat{2k}_{\mu} + r \sum_{\mu} \left(\frac{2}{a} - \widetilde{2k}_{\mu} \right) + 2m}{\widehat{2k}^2 + \left(r \sum_{\mu} \left(\frac{2}{a} - \widetilde{2k}_{\mu} \right) + 2m \right)^2} \right], \quad (11)$$

where $\widehat{k}^2 = \sum_{\mu} \widehat{k}_{\mu}^2$.

The complete form of the gluon propagator in the covariant gauge is quite complicated but can be found in Refs. [32, 33]. In this work we only need the gluon propagator up to order $\mathcal{O}(a^1)$

$$D_{g,\mu\nu}(k) = \frac{1}{\widehat{k}^2} \left[\delta_{\mu\nu} - (1 - \xi) \frac{a^2}{4} \widehat{k}_{\mu} \widehat{k}_{\nu} \right]. \quad (12)$$

We choose Feynman gauge $\xi = 1$ in this work. The quark-gluon-quark interaction vertex is given by [31]

$$V_{\alpha}^a(p_2, p_1, k) = -i g_s T^a \frac{a}{2} (\widehat{p_2 + p_1})_{\alpha} \gamma_{\alpha} - g_s T^a r \frac{a}{2} (\widehat{p_2 + p_1})_{\alpha} - i g_s T^a r c_{\text{SW}} \frac{a^2}{8} \widetilde{k}_{\alpha} \sum_{\mu} \sigma_{\alpha\mu} \widehat{2k}_{\mu}, \quad (13)$$

where $p_2 = p_1 + k$, the fermion momenta directions are assigned parallel to the direction of fermion line and k is the momentum of the gluon.

The naïve fermion action and Feynman rules are given by setting $r \rightarrow 0$ in the Wilson-Clover action and Feynman rules.

III. ONE-LOOP CORRECTIONS FOR QUASI-PDF

We now present the procedure for calculating within LPT the quasi-PDF in detail and the resulting quasi-PDF will be provided as an integrand of \mathbf{k}_{\perp} in analytical form to order $\mathcal{O}(a^0)$, and as an integrand of \mathbf{k}_{\perp} , k_4 to order $\mathcal{O}(a^1)$. We will discuss the collinear behavior of the quasi-PDF determined from LPT. As this work only concentrates on the unpolarized quark-in-quark PDF, quark-gluon mixing is not considered. The relevant Feynman diagrams at order $\mathcal{O}(\alpha_s a^0) + \mathcal{O}(\alpha_s a^1)$ are shown in Fig. 1. We have omitted those virtual correction diagrams (shown in Fig. 2) in our calculation, because their contributions to the quasi-PDF are proportional to $\delta(x - 1)$ and hence only contribute at $x = 1$.

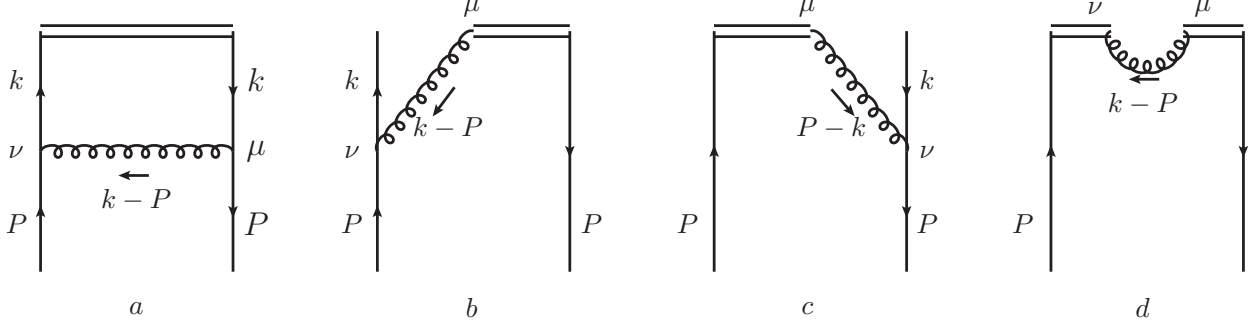


Figure 1: One-loop correction diagrams, the double line represents the gauge link in the quasi-PDF definition (3).

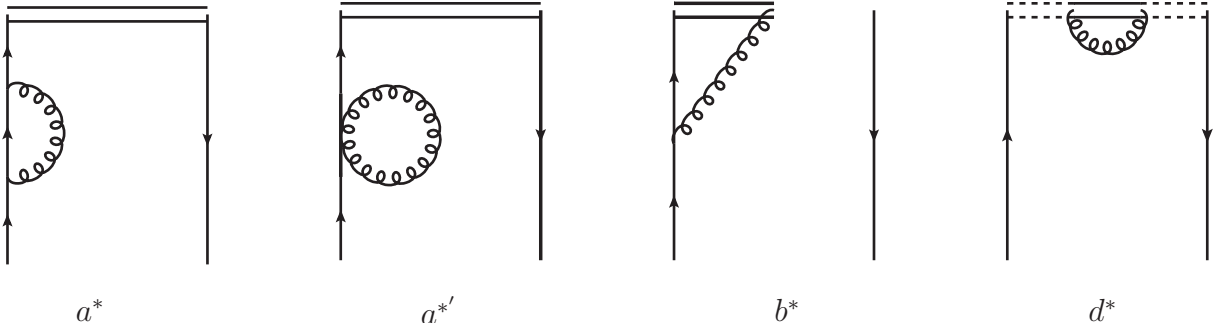


Figure 2: One-loop virtual correction diagrams of the quasi-PDF. They contribute to the quasi-PDF as $Z\delta(x-1)$, where Z is a x -independent constant. The quark self-energy diagram a^* (sunset) and $a^{*'}$ (tadpole) will contribute to the additive mass renormalization for Wilson fermions.

The one-loop Feynman diagrams lead to four terms,¹

$$\tilde{q}_a(x) = \int_{-\frac{\pi}{a}}^{\frac{\pi}{a}} \frac{d^4k}{(2\pi)^4} \frac{\sum_{\mu,\nu} \bar{U}(P) V_\mu(P, k, P-k) S_F(k) \gamma_3 S_F(k) V_\nu(k, P, k-P) U(P)}{\bar{U}(P) \gamma_3 U(P)} \times D_{g,\mu\nu}(P-k) \delta\left(x - \frac{k^3}{P^3}\right), \quad (14a)$$

¹ The one-loop corrections will induce a scalar fermion bilinear structure $\bar{U}(P)U(P)$, which can be related to the tree-level quasi-PDF fermion bilinear structure by $\bar{U}(P)U(P) = \Delta = \frac{\Delta}{\mathcal{P}_3} \bar{U}(P) \gamma_3 U(P)$, in which \mathcal{P}_μ and Δ is defined in Eq. (18b) (the continuum limit correspondence $\bar{u}(P)u(P) = 2m = \frac{m}{P^3} \bar{u}(P) \gamma^3 u(P)$ has been used in Ref. [14]). We see that this scalar bilinear term's contribution is at higher twist. The mixing is included by taking the trace of numerator and denominator on the right side of (14).

$$\begin{aligned} \tilde{q}_b(x) &= \int_{-\frac{\pi}{a}}^{\frac{\pi}{a}} \frac{d^4 k}{(2\pi)^4} \frac{\sum_{\mu\nu} \bar{U}(P) O_{1,\mu}(P, k, P-k) S_F(k) V_\nu(k, P, k-P) U(P)}{\bar{U}(P) \gamma_3 U(P)} \\ &\quad \times D_{g,\mu\nu}(P-k) \delta\left(x - \frac{k^3}{P^3}\right), \end{aligned} \quad (14b)$$

$$\begin{aligned} \tilde{q}_c(x) &= \int_{-\frac{\pi}{a}}^{\frac{\pi}{a}} \frac{d^4 k}{(2\pi)^4} \frac{\sum_{\mu\nu} \bar{U}(P) V_\mu(P, k, P-k) S_F(k) O_{1,\nu}(k, P, k-P) U(P)}{\bar{U}(P) \gamma_3 U(P)} \\ &\quad \times D_{g,\mu\nu}(P-k) \delta\left(x - \frac{k^3}{P^3}\right), \end{aligned} \quad (14c)$$

$$\tilde{q}_d(x) = \int_{-\frac{\pi}{a}}^{\frac{\pi}{a}} \frac{d^4 k}{(2\pi)^4} \frac{\sum_{\mu\nu} \bar{U}(P) O_{2,\mu\nu}(P, P, k-P) U(P)}{\bar{U}(P) \gamma_3 U(P)} D_{g,\mu\nu}(P-k) \delta\left(x - \frac{k^3}{P^3}\right). \quad (14d)$$

The momentum space gluon and gauge-link interaction terms can be obtained by Fourier transform of their corresponding coordinate expressions [19], leading to

$$O_{1,\mu}^A(q) = \frac{ig_s a T^A \gamma_3 \delta_{\mu 3}}{i\hat{q}_3}, \quad (15a)$$

$$O_{2,\mu\nu}^{AB}(p, p, q) = -g_s^2 a^2 \{T^A, T^B\} \gamma_3 \delta_{\mu 3} \delta_{\nu 3} \frac{1}{\hat{q}_3^2}. \quad (15b)$$

We note that there exists an extra $\mathcal{O}(a^1)$ terms in coordinate space,

$$g_s^2 \{T^A, T^B\} \gamma_3 \delta_{\mu 3} \delta_{\nu 3} e^{-ip_3 z} \left(\frac{z}{i\hat{q}_3} e^{\frac{z}{|z|} i \frac{aq_3}{2}} - \frac{a|z|}{2} \right). \quad (16)$$

This terms, however, is proportional to $\delta'(x-1)$ after the Fourier transformation (with respect to z) to x dependence and it is also excluded in the calculation since $\delta'(x-1)$ only contributes at $x=1$, similar to the virtual corrections.

The fermion propagator, gluon propagator and quark-gluon-quark vertex can be rewritten in short form for future convenience

$$S_F(k) = \frac{-i\mathcal{K} + \mathcal{M}}{\mathcal{K}^2 + \mathcal{M}^2}, \quad (17a)$$

$$D_{g,\mu\nu}(P-k) = \frac{\delta_{\mu\nu}}{Q^2}, \quad (17b)$$

$$V_\alpha^a(P, k, P-k) = -ig_s T^a \Lambda_\alpha \gamma_\alpha - ig_s T^a \Omega_\alpha - ig_s T^a \sum_\rho \sigma_{\alpha\rho} \widehat{2(P-k)}_\rho \Xi_\alpha. \quad (17c)$$

where we have defined

$$\mathcal{K}_\mu = \widehat{2k}_\mu, \quad \mathcal{M} = r \sum_\mu \left(\frac{2}{a} - \widehat{2k}_\mu \right) + 2m, \quad (18a)$$

$$\mathcal{P}_\mu = \widehat{2P}_\mu, \quad \Delta = r \sum_\mu \left(\frac{2}{a} - \widehat{2P}_\mu \right) + 2m, \quad (18b)$$

$$\mathcal{Q}_\mu = \widehat{k - P}_\mu, \quad \Lambda_\mu = \frac{a}{2} \widehat{k + P}_\mu, \quad (18c)$$

$$\Omega_\mu = \frac{ar}{2} \widehat{k + P}_\mu, \quad \Xi_\mu = r \frac{c_{\text{SW}} a^2}{8} \widehat{k - P}_\mu. \quad (18d)$$

The Feynman rules for naïve lattice fermion action corresponds to $r = 0$ limit of Eq. (17,18)

$$\Delta^{(0)} = \mathcal{M}^{(0)} = 2m, \quad (19a)$$

$$V_\alpha^{(0),a} = -igT^a \Lambda_\alpha \gamma_\alpha. \quad (19b)$$

We now perform calculations of the one-loop quark quasi-PDF with both the naïve lattice fermion action and Wilson-Clover fermion action, and discuss the impact of the Wilson-Clover term.

A. Quasi-PDF in naïve lattice fermion action

In the LPT quasi-PDF calculation, we use the same configuration as in Ref. [14]: the momentum of the parent quark is set to $P_\mu = (0, 0, P_3, P_4)$ and the transverse momentum UV cut-off is naturally chosen to be the lattice momentum cut-off $\pm\pi/a$. The relevant Feynman rules in naïve lattice fermion action reads:

$$S_F^{(0)}(k) = \frac{i\not{k} + \mathcal{M}^0}{\mathcal{K}^2 + (\mathcal{M}^0)^2}, \quad D_{g,\mu\nu}^{(0)}(P-k) = \frac{\delta_{\mu\nu}}{\mathcal{Q}^2}, \quad (20a)$$

$$V_\alpha^{(0),a}(P, k, P-k) = -ig_s T^a \Lambda_\alpha \gamma_\alpha, \quad \left[\sum_s U_s(P) \bar{U}_s(P) \right]^{(0)} = i\not{P} + \Delta^{(0)}. \quad (20b)$$

After some algebra, the one-loop correction diagrams give

$$\tilde{q}_a^{\text{nv}}(x) = \int_{-\frac{\pi}{a}}^{\frac{\pi}{a}} \frac{d^4 k}{(2\pi)^4} (-4g_s^2 C_F) P_3 \left\{ \frac{2\mathcal{K}_3 [\mathcal{P}_3 \mathcal{K}_3 (\Lambda^2 - 2\Lambda_3^2) + \Delta^{(0)} \mathcal{M}^{(0)} \Lambda^2] + 2\mathcal{P}_4 \mathcal{K}_3 \mathcal{K}_4 (\Lambda^2 - 2\Lambda_4^2)}{\mathcal{P}_3 \mathcal{Q}^2 [\mathcal{K}^2 + (\mathcal{M}^{(0)})^2]^2} - \frac{(\Lambda^2 - 2\Lambda_3^2)}{\mathcal{Q}^2 [\mathcal{K}^2 + (\mathcal{M}^{(0)})^2]} \right\} \delta(k_3 - xP_3), \quad (21a)$$

$$\tilde{q}_b^{\text{nv}}(x) = \tilde{q}_c^{\text{nv}}(x) = 2g_s^2 C_F \int_{-\frac{\pi}{a}}^{\frac{\pi}{a}} \frac{d^4 k}{(2\pi)^4} \frac{P_3 \Lambda_3 \mathcal{K}_4 \mathcal{P}_4 - \mathcal{K}_3 \mathcal{P}_3 + \Delta^{(0)} \mathcal{M}^{(0)}}{\mathcal{P}_3 \mathcal{Q}_3 \mathcal{Q}^2 [\mathcal{K}^2 + (\mathcal{M}^{(0)})^2]} \delta(k_3 - xP_3), \quad (21b)$$

$$\tilde{q}_d^{\text{nv}}(x) = -g_s^2 C_F \int_{-\frac{\pi}{a}}^{\frac{\pi}{a}} \frac{d^4 k}{(2\pi)^4} \frac{P_3}{\mathcal{Q}_3^2 \mathcal{Q}^2} \delta(k_3 - x P_3). \quad (21c)$$

The superscript nv denotes the quasi-PDF calculated in naïve fermion action. In the above equations, those terms odd under $k_{1,2} \rightarrow -k_{1,2}$ will not contribute to the integral and they are therefore already omitted.

In order to analytically integrate out k_4 , we introduce a variable change $z = a^{-2} e^{iak_4}$ [34, 35], then the k_4 -integration is transformed to a contour integral along the circle on the complex plane

$$\int_{-\frac{\pi}{a}}^{\frac{\pi}{a}} dk_4 f(k_4) = \frac{-i}{a} \oint_{|z|=a^{-2}} \frac{dz}{z} f\left(\frac{-i}{a} \ln(a^2 z)\right). \quad (22)$$

Under this transformation, the denominators of the quark and gluon propagators can be rewritten as

$$\mathcal{D}_F^{(0)} = \mathcal{K}^2 + (\mathcal{M}^{(0)})^2 = -a^{-2} z^{-2} (a^2 z^2 - \Gamma_+) (a^2 z^2 - \Gamma_-), \quad (23a)$$

$$\mathcal{D}_g^{(0)} = \mathcal{Q}^2 = -e^{-iaP_4} z^{-1} (z - \Pi_-) (z - \Pi_+). \quad (23b)$$

where Γ_{\pm} and Π_{\pm} are defined as

$$\Gamma_{\pm} = \frac{\kappa \pm \sqrt{\kappa^2 - \frac{4}{a^4}}}{2}, \quad \Pi_{\pm} = e^{iaP_4} \frac{\eta \pm \sqrt{\eta^2 - \frac{4}{a^4}}}{2}, \quad (24)$$

and

$$\kappa = \sum_{j=1}^3 \mathcal{K}_j^2 + (\mathcal{M}^{(0)})^2 + \frac{2}{a^2}, \quad \eta = \sum_{j=1}^3 \mathcal{Q}_j^2 + \frac{2}{a^2}. \quad (25)$$

The z -poles inside the integration circle $|z| = a^{-2}$ are $\pm\sqrt{\Gamma_-}/a$ and Π_- . The corresponding $k_4 = -ik^0$ poles reduce to the continuum k^0 poles on the upper complex plane in the $a \rightarrow 0$ limit

$$k_4^g = -\frac{i}{a} \log(a^2 \Pi_-) \rightarrow k_g^0 = P^0 - \sqrt{\mathbf{k}_{\perp}^2 + (k_3 - P_3)^2 + m^2 - i\epsilon}, \quad (26a)$$

$$k_4^{q,+} = -\frac{i}{a} \log(a\sqrt{\Gamma_-}) \rightarrow k_{q,+}^0 = -\sqrt{\mathbf{k}_{\perp}^2 + k_3^2 + m^2 - i\epsilon}, \quad (26b)$$

$$k_4^{q,-} = -\frac{i}{a} \log(-a\sqrt{\Gamma_-}) \rightarrow k_{q,-}^0 = \frac{i\pi}{a} - \sqrt{\mathbf{k}_{\perp}^2 + k_3^2 + m^2 - i\epsilon}, \quad (26c)$$

except for the second quark pole $k_4^{q,-}$, which turns out to present an unphysical continuum limit. However, the residue at this unphysical quark pole $\bar{k}_4^{q,-}$ vanishes in the continuum limit and the unphysical pole decouples in continuum limit. Applying the above transformation, the integral over k_4 is equivalent to taking the residue of the transformed integrand at $\bar{k}_0^{q,\pm}$, \bar{k}_4^g .

We have performed a Wick rotation $P_4 \rightarrow -iP^0$ (P^0 takes the value of r.h.s of Eq. (9)) in order to compare the quasi-PDF in LPT with the continuum quasi-PDF, which is calculated with Minkowski parent quark momentum P and loop momentum k . The impact of the Wick rotation will be discussed in a forthcoming paper [36].

It should be noticed that, in this work, the Wick rotation should take place after k_4 having been integrated out. One can see from the z poles in Eq. (24), if the Wick rotation is performed before taking residue at poles inside the integration circle $z = a^{-2}$, the gluon poles in Eq. (24) become

$$\frac{e^{iaP^4}}{2} \left(\eta \pm \sqrt{\eta^2 - \frac{4}{a^4}} \right) \rightarrow \frac{e^{aP^0}}{2} \left(\eta \pm \sqrt{\eta^2 - \frac{4}{a^4}} \right). \quad (27)$$

In this case, one can not ensure that the gluon poles are inside the integration circle due to the exponential factor e^{aP^0} being larger than one, thus as a consequence, the residue at the gluon pole may not be included in the integration and it leads to incorrect results. The kinematic region which constrains the Wick-rotated gluon pole (Π_- with $P_4 \rightarrow -iP^0$) inside the integration circle $z = a^{-2}$ can be evaluated by

$$\frac{e^{aP^0}}{2} \left(\eta - \sqrt{\eta^2 - \frac{4}{a^4}} \right) < \frac{1}{a^2}. \quad (28)$$

Expanding to $\mathcal{O}(a^1)$ gives

$$1 + a \left(\sqrt{m^2 + P_3^2} - \sqrt{\mathbf{k}_\perp^2 + P_3^2(1-x)^2} \right) < 1 \Rightarrow \mathbf{k}_\perp^2 > m^2 + x(2-x)P_3^2. \quad (29)$$

For the region $\mathbf{k}_\perp^2 < m^2 + x(2-x)P_3^2$, as discussed in Ref. [27], one needs to consider another piece of integration to recover the correct integral. It is due to the gluon pole crossing the integration circle. The condition in Eq. (29), which determines the position of gluon pole, is only an $\mathcal{O}(a^1)$ approximation to the exact condition (Eq.(28)) in LPT. The exact condition in LPT is hard to solve, thus in our quasi-PDF calculation, we apply the Wick rotation $P_4 \rightarrow -iP^0$ after k_4 being integrated out to avoid the complexity.

The following contents of this paper are based on the k_4 -integrated out results (except Sec. III C, the quasi-PDF calculated with Wilson-Clover action), that means that we have already performed the Wick rotation $P_4 \rightarrow -iP^0$ after the k_4 integration unless specified.

The expressions of the k_4 integration in Eq. (14) are very lengthy and they do not provide any insight to the discussion here. We therefore provide these expressions in appendix A, see Eqs. (A1,A3,A4).

B. Continuum limit and collinear behavior of quasi-PDF in naïve lattice fermion action

The continuum limit of Eqs. (A1,A3,A4) can be calculated directly by performing the Wick rotation $P_4 \rightarrow -iP^0$ and the $a \rightarrow 0$ limit. The result turns out to be identical to the \mathbf{k}_\perp -unintegrated quasi-PDF calculated directly in the continuum. We will show the equivalence later in the example calculation of $\tilde{q}_b^{\text{nv}}(x)$.

There is a major difference between the quasi-PDF calculated by LPT and the continuum quasi-PDF: The collinear divergence is absent in the LPT-calculated quasi-PDF when the lattice spacing a is finite, even after performing the Wick rotation $P_4 \rightarrow -iP^0$.

The reason is that the lattice artifacts from the finite lattice spacing have regulated the collinear divergence. The absence of collinear divergence can be verified in the numerical results by setting the quark mass to zero, see Fig. 5. It can also be seen in the analytical \mathbf{k}_\perp -integrand of the quasi-PDF in LPT. We take the calculation of diagram *b* as an example to present the continuum limit and illustrate how to extract the collinear behavior in lattice perturbation calculation.

The continuum correspondence of $\tilde{q}_b^{\text{nv}}(x)$ is

$$[\tilde{q}_b(x)]_{\text{cont.}} = \int d^4k \frac{g_s^2 C_F}{(2\pi)^4} \frac{\bar{U}(P) \gamma^z (\not{k} + m) \gamma^z U(P)}{(P^z - k^z)(P - k)^2(k^2 - m^2)} \delta\left(x - \frac{k^z}{P^z}\right) / [\bar{U}(P) \gamma^z U(P)] \quad (30)$$

The k^0, k^z -integration gives exactly the same result as $a \rightarrow 0$ limit of the lattice perturbation result (A3)

$$\begin{aligned} & \lim_{a \rightarrow 0} \tilde{q}_b^{\text{nv}}(x, \mathbf{k}_\perp) \\ &= \frac{\alpha_s C_F}{8\pi^3 P_3 (1-x)} \left[-\frac{P_0 \sqrt{\mathbf{k}_\perp^2 + m^2 + P_3^2 x^2} + m^2 - P_3^2 x}{\sqrt{\mathbf{k}_\perp^2 + m^2 + P_3^2 x^2} P_0 \sqrt{\mathbf{k}_\perp^2 + m^2 + P_3^2 x^2} + m^2 + P_3^2 x} \right. \\ & \quad \left. + \frac{\left(P_0 \left(\sqrt{\mathbf{k}_\perp^2 - m^2 + P_3^2 (x-2)x + P_0^2} - P_0 \right) + m^2 - P_3^2 x \right)}{\sqrt{\mathbf{k}_\perp^2 - m^2 + P_3^2 (x-2)x + P_0^2} \left(P_0 \left(\sqrt{\mathbf{k}_\perp^2 - m^2 + P_3^2 (x-2)x + P_0^2} - P_0 \right) + m^2 + P_3^2 x \right)} \right]. \quad (31) \end{aligned}$$

The continuum quasi-PDF can be obtained by integrating out \mathbf{k}_\perp , where we already performed the expansion $m \rightarrow 0$. It clearly shows that there exists a collinear divergence in the region $0 < x < 1$

$$[\tilde{q}_b(x)]_{\text{cont.,col.}} = \begin{cases} -\frac{g_s^2 C_F}{8\pi^2} \frac{2x}{1-x} \ln m^2 + \dots & 0 < x < 1 \\ \dots & x < 0 \text{ or } x > 1 \end{cases} \quad (32)$$

where the ellipsis denotes those terms which do not contain a collinear divergence (at the order of $\mathcal{O}(m^0)$).

Physically, the collinear divergence happens when the split quark's momentum \mathbf{k} is parallel to the parent quark's momentum \mathbf{P} , or equivalently $\mathbf{k}_\perp = \mathbf{0}$. To extract the collinear behavior of the LPT-calculated quasi-PDF, we expand the numerator and denominator of Eq. (A3) around $|\mathbf{k}_\perp| = 0$. The expansion takes the form

$$\lim_{\mathbf{k}_\perp \rightarrow \mathbf{0}} \tilde{q}^{\text{nv}}(x, \mathbf{k}_\perp) = \sum_{i=1}^3 \frac{\mathcal{N}_{b,i}^{(0)}}{\mathcal{D}_{b,i}^{(0)} + \mathcal{D}_{b,i}^{(1)} \mathbf{k}_\perp^2}, \quad (33)$$

in which $i = 1, 2, 3$ denotes the 1st, 2nd, 3rd term in (A3) corresponding to the gluon pole, quark pole and unphysical quark pole's residue. The expressions for $\mathcal{N}_{i,b}^{(n)}$ and $\mathcal{D}_{i,b}^{(n)}$ are

$$\mathcal{N}_{b,1}^{(0)} = ia^3 P_3 \Delta_\Pi g_s^2 C_F \frac{\cos\left(\frac{aP_3}{2}(x+1)\right)}{\sin\left(\frac{aP_3}{2}(x-1)\right)} \left[\frac{2ia^2 m^2 \Delta_\Pi + (\Delta_\Pi^2 - 1) \sin(aP_4)}{\sin(aP_3)} - \frac{2i \Delta_\Pi}{\csc(aP_3 x)} \right], \quad (34a)$$

$$\mathcal{D}_{b,1}^{(0)} = 16\pi^3 \sqrt{\mathcal{R}_\Pi^2 - 1} (\Delta_\Pi^4 - 2\Delta_\Pi^2 \mathcal{R}_\Gamma + 1), \quad (34b)$$

$$\mathcal{D}_{b,1}^{(1)} = 32\pi^3 a^2 \Delta_\Pi^2 (\mathcal{R}_\Gamma - \Delta_\Pi^2) + \frac{8\pi^3 a^2 (8\Delta_\Pi^2 (1 - \mathcal{R}_\Pi^2) + \mathcal{R}_\Pi (\Delta_\Pi^4 - 2\Delta_\Pi^2 \mathcal{R}_\Gamma + 1))}{\sqrt{\mathcal{R}_\Pi^2 - 1}}, \quad (34c)$$

$$\mathcal{N}_{b,2}^{(0)} = a^3 P_3 e^{iaP_4} g_s^2 C_F \frac{\cos\left(\frac{aP_3}{2}(x+1)\right)}{\sin\left(\frac{aP_3}{2}(x-1)\right)} \left[-\frac{2a^2 m^2 \sqrt{\Delta_\Gamma} + i(1-\Delta_\Gamma) \sin(aP_4)}{\sin(aP_3)} + 2\sqrt{\Delta_\Gamma} \sin(aP_3 x) \right], \quad (35a)$$

$$\mathcal{D}_{b,2}^{(0)} = 32\pi^3 \sqrt{\mathcal{R}_\Gamma^2 - 1} \left(-2e^{iaP_4} \sqrt{\Delta_\Gamma} \mathcal{R}_\Pi + e^{2iaP_4} + \Delta_\Gamma \right), \quad (35b)$$

$$\mathcal{D}_{b,2}^{(1)} = \frac{32\pi^3 a^2}{\sqrt{\mathcal{R}_\Gamma^2 - 1}} \left[2e^{iaP_4} \sqrt{\Delta_\Gamma} \sqrt{\mathcal{R}_\Gamma^2 - 1} \mathcal{R}_\Pi - e^{iaP_4} \sqrt{\Delta_\Gamma} (4\mathcal{R}_\Gamma \mathcal{R}_\Pi + \mathcal{R}_\Gamma^2 - 1) + 2e^{2iaP_4} \mathcal{R}_\Gamma + 2\Delta_\Gamma^2 \right]. \quad (35c)$$

Here, we have omitted the unphysical quark pole ($i = 3$) because it is of $\mathcal{O}(a^2)$ in the lattice spacing and does not contain any collinear divergence. The definitions of $\mathcal{R}_{\Gamma,\Pi}$ and $\Delta_{\Gamma,\Pi}$ are

$$\mathcal{R}_\Pi = \frac{1}{2} \left(\sqrt{\frac{\Pi_-}{\Pi_+}} + \sqrt{\frac{\Pi_+}{\Pi_-}} \right) \Big|_{\mathbf{k}_\perp=0}, \quad \mathcal{R}_\Gamma = \frac{1}{2} \left(\sqrt{\frac{\Gamma_-}{\Gamma_+}} + \sqrt{\frac{\Gamma_+}{\Gamma_-}} \right) \Big|_{\mathbf{k}_\perp=0}, \quad (36a)$$

$$\Delta_\Pi = e^{iaP_4} \left(\mathcal{R}_\Pi - \sqrt{\mathcal{R}_\Pi^2 - 1} \right), \quad \Delta_\Gamma = \mathcal{R}_\Gamma - \sqrt{\mathcal{R}_\Gamma^2 - 1}. \quad (36b)$$

The \mathbf{k}_\perp -integration of $\mathcal{N}_{b,i}^{(0)} / (\mathcal{D}_{b,i}^{(0)} + \mathcal{D}_{b,i}^{(1)} \mathbf{k}_\perp^2)$ leads to

$$\int_0^\mu d^2 \mathbf{k}_\perp \frac{\mathcal{N}_{b,i}^{(0)}}{(\mathcal{D}_{b,i}^{(0)} + \mathcal{D}_{b,i}^{(1)} \mathbf{k}_\perp^2)} = \pi \frac{\mathcal{N}_{b,i}^{(0)}}{\mathcal{D}_{b,i}^{(1)}} \ln \frac{\mu^2 \mathcal{D}_{b,i}^{(1)}}{\mathcal{D}_{b,i}^{(0)}}, \quad (37)$$

where μ is a finite scale which does not affect the IR behavior of the integral. It straightforward to check that $\mathcal{D}_{b,i}^{(0)}$ is nonzero when $m \rightarrow 0$ with finite lattice spacing a . Consequently, the collinear divergence is regularized by $\mathcal{D}_{b,i}^{(0)}$. We have calculated the quasi-PDF numerically with explicit $m = 0$ as shown in Fig.5 and there is no signal of a collinear divergence in the whole x region. If we take the continuum limit before the expansion around $m = 0$, we have

$$\lim_{m \rightarrow 0} \left(\lim_{a \rightarrow 0} \pi \frac{\mathcal{N}_{b,1}^{(0)}}{\mathcal{D}_{b,1}^{(1)}} \ln \frac{\mu^2 \mathcal{D}_{b,1}^{(1)}}{\mathcal{D}_{b,1}^{(0)}} \right) = \begin{cases} -\frac{g_s^2 C_F}{8\pi^2} \frac{2x}{1-x} \ln m^2 + \dots & x < 1 \\ \dots & x > 1 \end{cases} \quad (38)$$

Through the above procedure, we can extract the collinear behavior of the 2nd term in (A3), which reads

$$\lim_{m \rightarrow 0} \left(\lim_{a \rightarrow 0} \pi \frac{\mathcal{N}_{b,2}^{(0)}}{\mathcal{D}_{b,2}^{(1)}} \ln \frac{\mu^2 \mathcal{D}_{b,2}^{(1)}}{\mathcal{D}_{b,2}^{(0)}} \right) = \begin{cases} \frac{g_s^2 C_F}{8\pi^2} \frac{2x}{1-x} \ln m^2 + \dots & x < 0 \\ \dots & x > 0 \end{cases} \quad (39)$$

To sum up, the collinear divergence of $\tilde{q}_b(x)$ is

$$\sum_{i=1}^2 \lim_{m \rightarrow 0} \left(\lim_{a \rightarrow 0} \pi \frac{\mathcal{N}_{b,i}^{(0)}}{\mathcal{D}_{b,i}^{(0)}} \ln \frac{\mu^2 \mathcal{D}_{b,i}^{(1)}}{\mathcal{D}_{b,i}^{(0)}} \right) = \begin{cases} -\frac{g_s^2 C_F}{8\pi^2} \frac{2x}{1-x} \ln m^2 + \dots & 0 < x < 1 \\ \dots & x < 0 \text{ or } x > 1 \end{cases} \quad (40)$$

and it is identical to the collinear divergence of the continuum quasi-PDF in (32). The above example calculation has shown that in order to recover the collinear divergence in continuum quasi-PDF, one needs to eliminate the effect of the finite lattice spacing by taking $a \rightarrow 0$ limit before the expansion around $m = 0$. Eqs. (38,39,40) show that the collinear divergence originates from the gluon pole $i = 1$ in the region $0 < x < 1$. We further expand $\mathcal{D}_{b,1}^{(0)}/\mathcal{D}_{b,1}^{(1)}$ to $\mathcal{O}(a^2)$ (in the region $0 < x < 1$, there is no collinear divergence in region $x < 0 \vee x > 1$) in order to study how lattice artifacts affect the collinear behavior

$$\lim_{a \rightarrow 0} \ln \frac{\mu^2 \mathcal{D}_{b,1}^{(0)}}{\mathcal{D}_{b,1}^{(0)}} \stackrel{P_3 \gg m}{\approx} \ln \frac{\mu^2}{\frac{1}{2} a^2 P_3^4 \left[x(x^2 - 1)^2 + \mathcal{O}\left(\frac{m^2}{P_3^2}\right) \right] + m^2(x-1)^2}. \quad (41)$$

Therefore, the correct limit to recover the logarithmic collinear divergence is $aP_3^2 \approx m$ and $m \ll P_3$. The first condition $aP_3^2 \approx m$ matches the lattice artifacts with the collinear regulator m^2 , since, assuming $aP_3^2 = \lambda m$ with λ being a finite constant, gives

$$\ln \frac{\mu^2}{\frac{1}{2} a^2 P_3^4 \left[x(x^2 - 1)^2 \right] + m^2(x-1)^2} = \ln \frac{\mu^2}{m^2} - \ln \left[(x-1)^2 + x(x^2 - 1)^2 \frac{\lambda^2}{2} \right] \quad (42)$$

and the collinear divergent part $\ln(\mu^2/m^2)$ stays the same as long as aP_3^2 and m are of the same order. This condition also indicates $aP_3 \ll 1$ and it eliminates the subleading order lattice artifacts (e.g. $a^3 m^2 P_3^3$, $a^4 P_3^6$). The second condition $m \ll P_3$ justifies m as a collinear regulator. The limit to fully recover the quasi-PDF calculated in continuum QCD is $aP_3^2 \ll m \ll P_3$, in which the first condition allows us to drop the lattice artifacts completely

$$\ln \frac{\mu^2}{\frac{1}{2} a^2 P_3^4 \left[x(x^2 - 1)^2 \right] + m^2(x-1)^2} \xrightarrow{aP_3^2 \ll m \ll P_3} \ln \frac{\mu^2}{m^2(1-x)^2}. \quad (43)$$

We can also see that the effects of lattice artifacts are getting enhanced for large P_3 . We will further justify this conclusion in the numerical calculations, see Sec.IV.

C. One-loop quasi-PDF in Wilson-Clover lattice fermion action

The calculation (k_4 -integration) of the quasi-PDF in Wilson-Clover action is analogous to the naïve lattice fermion calculation, however, the analytical k_4 -integration in Wilson-Clover lattice fermion case are too cumbersome to be displayed (and again do not provide any insight to our present discussion), hence we only briefly introduce the procedure of k_4 -integration. (we do not apply the Wick rotation $P_4 \rightarrow -iP^0$ in this subsection, because k_4 has not been integrated out).

In the case of Wilson-Clover lattice fermion action, there are in total four poles of $z =$

$a^{-2}e^{iak_4}$ in the quark propagator (11):

$$z_{\lambda_1, \lambda_2} = \frac{1}{2} \left\{ \frac{r \left(-2am - 8r + ar \sum_{i=1}^3 \widetilde{2k}_i \right) + \lambda_2 \sqrt{\Phi}}{a^2 (1 - r^2)} + \lambda_1 \left[-\frac{2}{a^4} + \frac{2r \left(-2am - 8r + ar \sum_{i=1}^3 \widetilde{2k}_i \right)}{a^4 (1 - r^2)^2} \right. \right. \\ \left. \left. \times \left(r \left(-2am - 8r + ar \sum_{i=1}^3 \widetilde{2k}_i \right) + \lambda_2 \sqrt{\Phi} \right) + \frac{\Phi + a^2 r^2 \sum_{i=1}^3 \widetilde{2k}_i^2 + 6r^2 - 2}{a^4 (1 - r^2)} \right]^{\frac{1}{2}} \right\}, \quad (44)$$

where $\lambda_1 = \pm 1$ and $\lambda_2 = \pm 1$ and

$$\Phi = 4 + 4a^2 m^2 + 32amr + 60r^2 + a^2 r^2 \widetilde{2k}_\perp^2 - 4ar(am + 4r) \widetilde{2k}_3 + a^2 r^2 \widetilde{2k}_3^2 \\ + 2ar \sum_{i=1}^2 \widetilde{2k}_i \left(-2am - 8r + ar \widetilde{2k}_3 \right) + 2a^2 r^2 \widetilde{2k}_1 \widetilde{2k}_2 + a^2 (1 - r^2) \widetilde{2k}^2. \quad (45)$$

where $\widetilde{2k}_\perp^2 = \sum_{i=1}^2 \widetilde{2k}_i^2$ and $\widetilde{2k}^2 = \sum_{i=1}^3 \widetilde{2k}_i^2$. In the $r \rightarrow 0$ limit, $|z_{\pm 1, \mp 1}|$ become larger than a^{-2} and are therefore excluded from the integration, while $z_{\pm 1, \mp 1}$ reduce to the z pole in Eq.(23a), i.e. the naïve fermion action result. The z poles of gluon propagator: Π_\pm in eq. (24) are unchanged.

For $r > 0$, the z -poles inside the integration circle $|z| = a^{-2}$ are $z_{\mp 1, \pm 1}$ and $z = \Pi_-$. Taking the residue of eq. (14) at the above mentioned poles gives the k_4 -integration of one-loop quasi-PDF in Wilson-Clover lattice fermion action.

It should be noted that after the k_4 integration, $\tilde{q}_d(x)$ is independent of r and quark mass m . Therefore this quantity is the same for both the naïve fermion action and Wilson-Clover fermion action cases and we only present the numerical results of $\tilde{q}_d(x)$ with naïve fermion action.

IV. NUMERICAL RESULTS

After analytically integrating out k_3, k_4 and applying the Wick rotation $P_4 \rightarrow -iP^0$ to Eqs. (A1,A3,A4), the transverse momentum \mathbf{k}_\perp integration is performed through a two-dimensional numerical integration. The k -integrated quasi-PDF actually only depends on three dimensionless quantities: x, am and aP_3 . However, in order to explore how the quasi-PDF calculated by lattice perturbation theory evolves with respect to a, m and P_3 , we still keep them as independent parameters. The lattice spacing is chosen as $a = 2^n \text{ fm}$ for $n = -11, -10, -8, -4, -3, -2, -1$, the parent quark's longitudinal momentum is $P_3 = 1.5\pi \text{ fm}^{-1}$ and bare quark mass is set to $m = 0.5\pi \text{ fm}^{-1}$ or $m = 0.005\pi \text{ fm}^{-1}$ to explore the collinear behavior of the quasi-PDF. We also calculated the numerical results of quasi-PDF in LPT for the vanishing bare quark mass case together with bare quark mass m set to the one-loop result for the critical mass of Wilson-Clover fermions, in order to confirm the absence of a collinear divergence. We have omitted the quasi-PDF in the region $0.6 < x < 1.4$ in order to avoid the divergent terms such as $(1-x)^{-1}$ and $(1-x)^{-2}$ which will become overwhelming compared to other x regions. We separate the contribution from diagrams $a, b, c, \tilde{q}_{a,b,c}(x)$, and diagram $d, \tilde{q}_d(x)$, because $\tilde{q}_d(x)$ is linearly UV divergent and also contains a quadratic

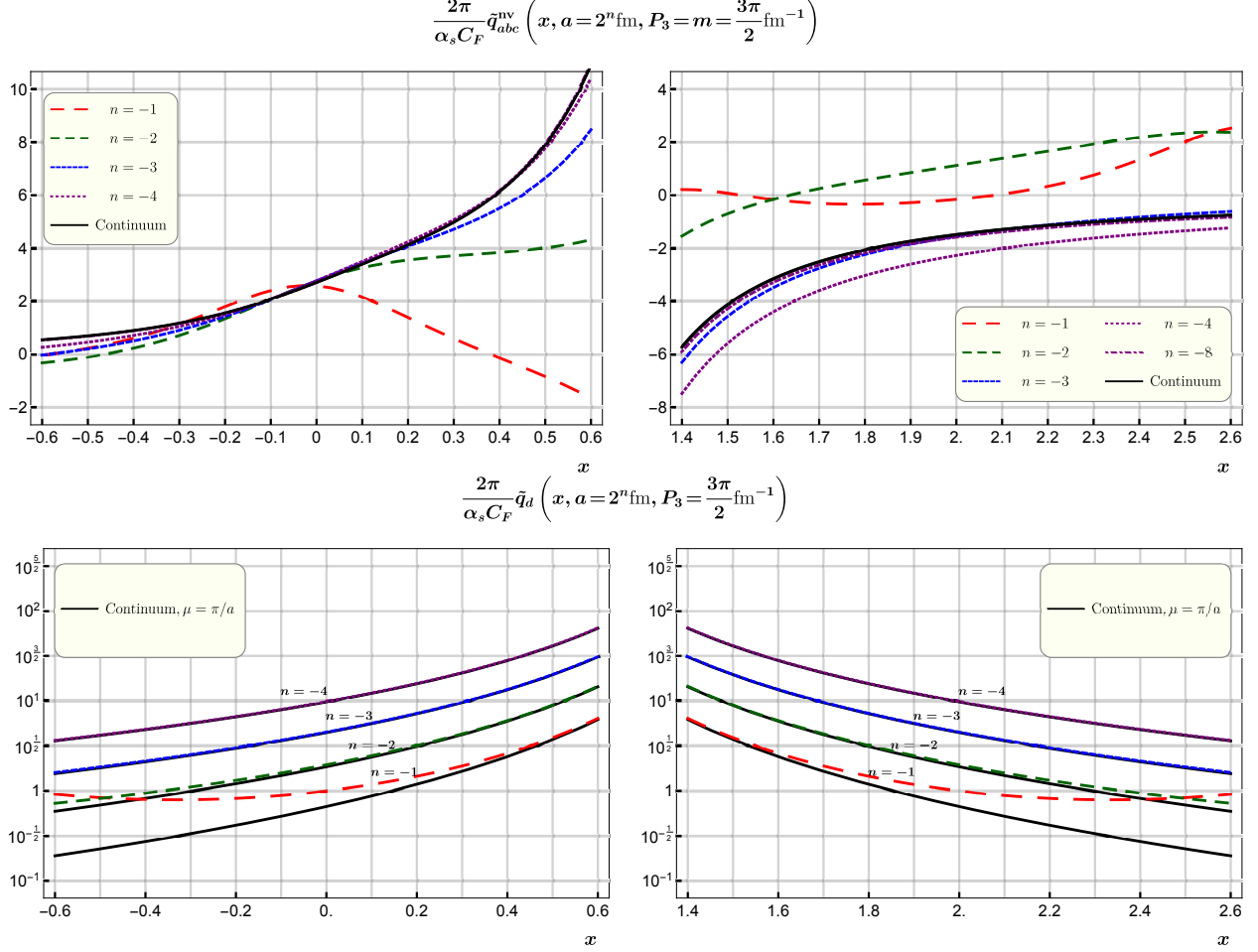


Figure 3: quasi-PDF in naïve lattice fermion formulation, with different lattice spacing. The quasi-PDF in LPT approaches the continuum quasi-PDF when the lattice spacing is small enough.

pole, i.e. $(1-x)^{-2}$. The $\tilde{q}_d(x)$ contribution to the quasi-PDF is much larger than $\tilde{q}_{a,b,c}(x)$. In such a case, the information of $\tilde{q}_{a,b,c}(x)$ will be overwhelmed by $\tilde{q}_d(x)$ if the two parts are summed together. Furthermore, the collinear behavior of $\tilde{q}_{a,b,c}(x)$ and $\tilde{q}_d(x)$ is also quite different in the continuum quasi-PDF: the former one carries collinear divergence in the region $0 < x < 1$ while the latter one is free of collinear divergence. For those reasons, we present the numerical results of $\tilde{q}_{a,b,c}(x)$ and $\tilde{q}_d(x)$ separately. For the numerical calculation with Wilson-Clover fermion, the Wilson parameter is set to $r = 1/2$ and $c_{\text{SW}} = 1$ for the leading order Clover parameter.

The continuum quasi-PDF can be found in Ref. [14]. The numerical results with different lattice spacing and comparison to the continuum quasi-PDF are shown in Fig.3. There are 4 different curves for the continuum quasi-PDF $\tilde{q}_d(x)$, corresponding to the linear UV divergence in continuum quasi-PDF with the transverse momentum cut-off $\Lambda = \pi/a$. As a consequence, different lattice spacings result in different continuum quasi-PDFs. The $\tilde{q}_{a,b,c}(x)$ are UV finite, therefore there is only one continuum limit. We use \tilde{q}^{nv} to denote the quasi-PDF calculated in naïve fermion action and \tilde{q}^{WC} to denote the quasi-PDF calculated in Wilson-Clover fermion action.

A. Numerical results of quasi-PDF in naïve lattice fermion action

From Fig. 3 we find that when the lattice spacing is small enough, the quasi-PDF in naïve lattice fermion action ($\tilde{q}^{\text{nv}}(x)$) closely approaches the continuum quasi-PDF. For the region $x > 1$, the $\tilde{q}_{a,b,c}^{\text{nv}}(x)$ with $n = -4$ curve appears to be further away from the continuum quasi-PDF than the $n = -3$ curve. However, this is a coincidence, since as the lattice spacing further shrinks to $n = -8$, it approaches the continuum quasi-PDF much closer than $n = -3, -4$. $\tilde{q}_d^{\text{nv}}(x)$ is symmetric with respect to $x = 1$ and it converges to the corresponding continuum quasi-PDF from diagram d faster than $\tilde{q}_{a,b,c}^{\text{nv}}(x)$. Indeed, when $a = 2^{-3}\text{fm}$, $q_d(x)$ almost coincides with the continuum quasi-PDF. The $\mathcal{O}(a^0)$ integrand of diagram d in (21c) reads

$$\mathcal{Q}_3^{-2} \mathcal{Q}^{-2} = \left(\frac{a}{2}\right)^4 \left[\sin\left(a \frac{P_3 - k_3}{2}\right) \right]^{-2} \sum_{\mu} \left[\sin\left(a \frac{P_{\mu} - k_{\mu}}{2}\right) \right]^{-2}, \quad (46)$$

which is an even function in $(1 - x)$. The $a \rightarrow 0$ series expansion gives the continuum integrand $(P_3 - k_3)^{-2} (P - k)^{-2}$ with residual term at $\mathcal{O}(a^2)$, while the difference between lattice perturbation and continuum integrand of $q_{a,b,c}^{\text{nv}}(x)$ is of order $\mathcal{O}(a^1)$. Therefore, the contribution from diagram d approaches its continuum correspondence faster than the contributions from diagrams a, b and c .

We also calculated the quasi-PDF with quark mass $m = 0.02\pi/L$ to study the different collinear behavior in LPT-calculated quasi-PDF and continuum quasi-PDF. The numerical result is shown in Fig. 4. The lattice perturbation result $\tilde{q}^{\text{nv}}(x)$ still coincides with the continuum quasi-PDF in the region $x < 0$ (and $x > 1$ which is not shown here), because there is no collinear divergence in the two regions. Consequently, the small quark mass limit and small lattice spacing limit commute in the lattice perturbation quasi-PDF. In the region $0 < x < 1$ there is a significant discrepancy, because there is a collinear divergence term $(1 + x^2) \ln m^2 / (x - 1)$ [14] while the collinear divergence is absent in LPT-calculated quasi-PDF due to the finite lattice spacing. However, if we take $a \rightarrow 0$ faster than $m \rightarrow 0$ (the purple dot-dashed line, almost overlapping with the continuum), the collinear divergence actually begins to show up in the region $0 < x < 1$. Since there is no collinear divergence both in the continuum and lattice perturbation calculated quasi-PDF $\tilde{q}_d(x)$, they always agree nicely when the lattice spacing a is smaller than 2^{-3}fm . An extreme case is to set the quark mass to zero as shown in Fig. 5. For nonzero lattice spacing, the lattice perturbation calculated quasi-PDF (contribution from diagrams a, b and c) are free from the collinear divergence in the region $0 < x < 1$.

It should be noted that the lattice spacing a and quark mass m have different dimensions, thus it is not meaningful to compare how fast a and m approach zero directly; rather, one should compare the dimensionless quantities aP_3 and m/P_3 . The continuum limit should be understood as $aP_3 \ll m/P_3$, in other words, a approaches zero much faster than m . In Fig.6, we compare the lattice perturbation quasi-PDF and continuum quasi-PDF (contains collinear divergence $\ln m$) with fixed lattice spacing $a = 2^{-10}\text{fm}$ and $m = 0.005\pi\text{fm}^{-1}$ but for different quark momenta $P_3 = 1.5n\pi\text{fm}^{-1}$ for $n = 0.5, 1, 2, 4$. The values of $aP_3^2/m = 0.345, 1.381, 5.524, 22.089$ correspondingly demonstrate the transition from $aP_3 \ll m/P_3$ to $aP_3 \gg 1$. From the figure we find that in the region $x < 0$ which does not contain any collinear divergence, the quasi-PDF in LPT always shows good agreement with the continuum quasi-PDF, while in the region $0 < x < 1$ where the continuum

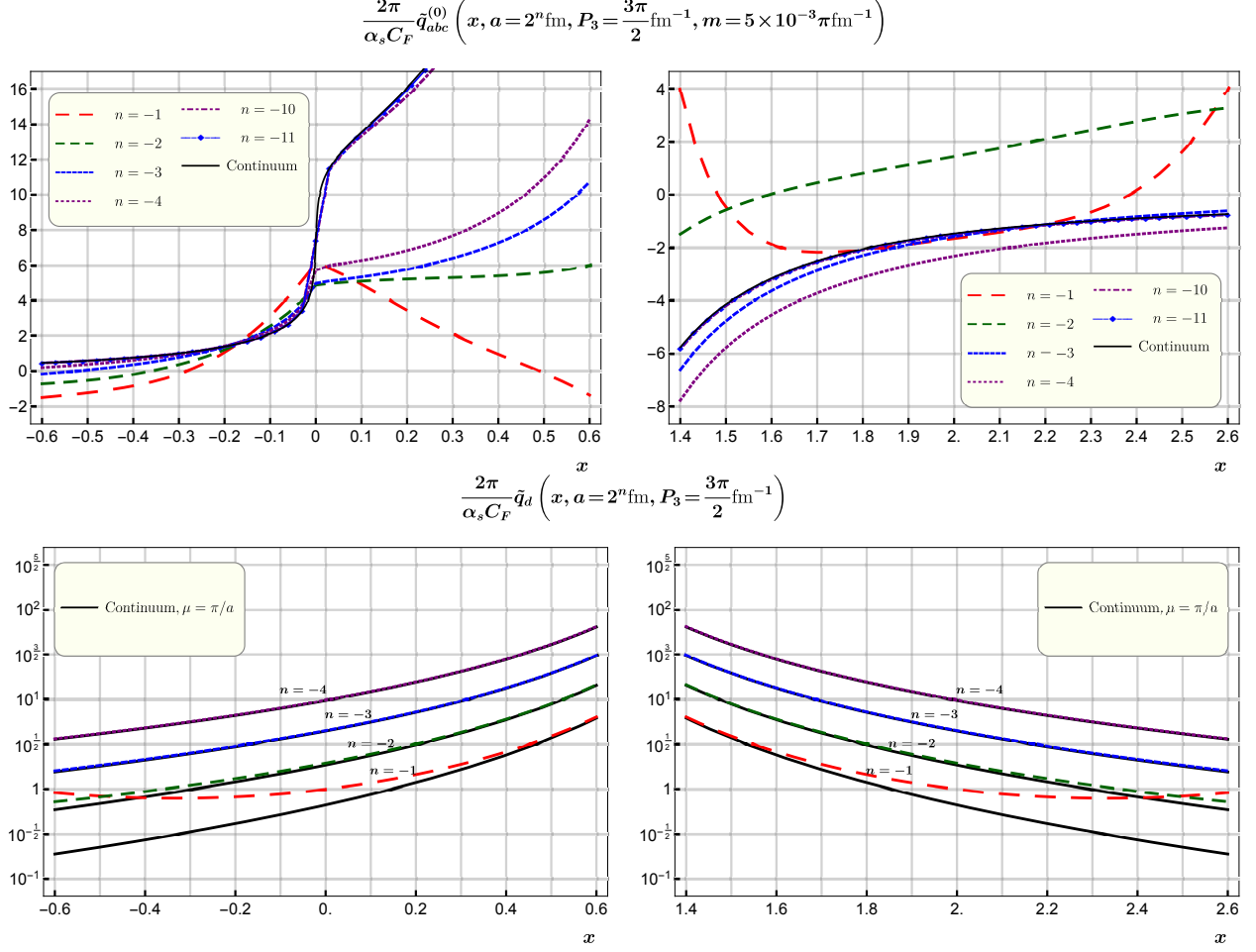


Figure 4: Numerical results for the quasi-PDF with a small quark mass and different lattice spacings. The quasi-PDF in LPT does not agree well with the continuum quasi-PDF when the collinear divergence appears in continuum quasi-PDF.

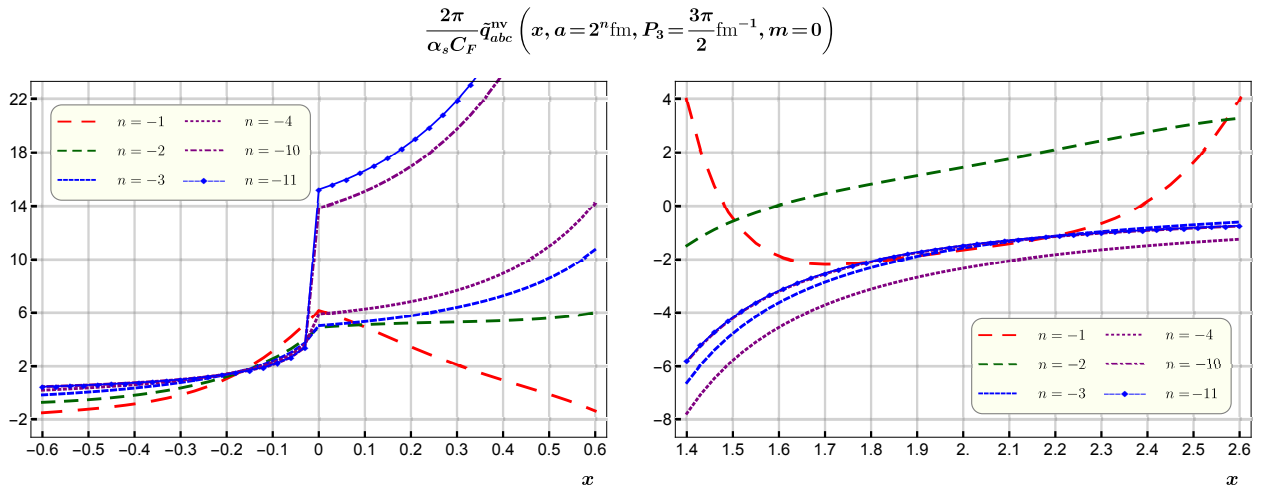


Figure 5: quasi-PDF in LPT with massless quarks. There is no collinear divergence ($\log m^2$) when the lattice spacing is nonzero.

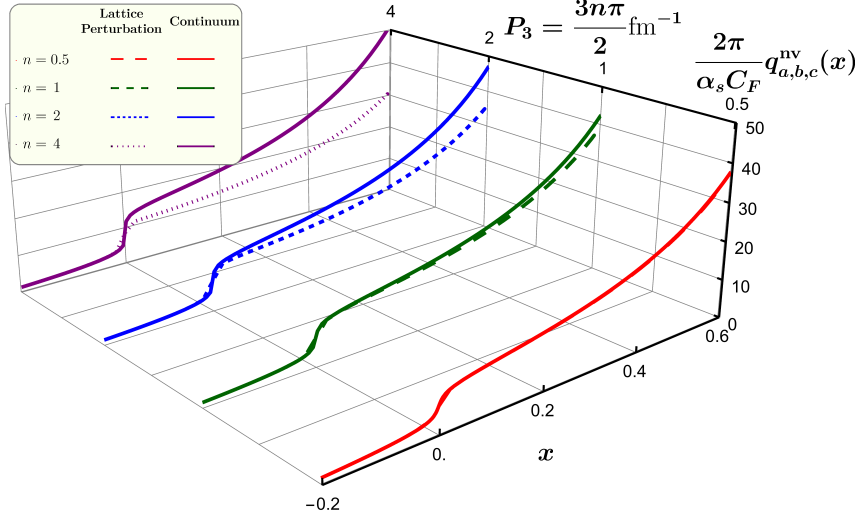


Figure 6: Numerical results for the quasi-PDF (naïve fermion action case) with different quark momentum P_3 (fixed lattice spacing and quark mass). The increasing P_3 changes the order of aP_3^2 and m from $aP_3^2 \ll m$ to $aP_3^2 \gg m$, resulting in the discrepancy between lattice perturbation and continuum quasi-PDF.

quasi-PDF contains a collinear divergence, the discrepancy between lattice perturbation quasi-PDF and continuum quasi-PDF increases with increasing P_3 . This is because increasing P_3 will enhance the effect from lattice artifacts, i.e. aP_3 and aP_4 as analysed analytically in Sec. III B. As a consequence, the implementation of the target mass correction [17] to eliminate P_3 power suppressed corrections becomes quite essential, otherwise one has to pay the price of large lattice artifacts when performing lattice QCDs simulation with large values of P_3 .

B. Numerical results of quasi-PDF in Wilson-Clover lattice fermion action

We also calculated the quark quasi-PDF in Wilson-Clover action with both massive and massless quark. The Wilson parameter is set as $r = 1/2$ and the Clover parameter is chosen to be the leading order in perturbation theory: $c_{\text{sw}} = 1$. The numerical results are shown in Fig. (7,8).

It is worth mentioning that the Wilson-Clover fermion receives an additive mass corrections from renormalization, which means the bare quark mass (critical mass) can be initially negative (which is the case in LQCD calculations) in order to have a vanishing renormalized quark mass. We also calculated the quasi-PDF with the bare quark mass set to the one-loop critical mass calculated from the quark self-energy diagram (sunset diagram and tadpole diagram). We follow Ref. [37], but with $r = 1/2$ and $c_{\text{sw}} = 1$)², the resulting critical mass is $am_0(c_{\text{sw}}=1, r=1/2) = -0.288C_F g_s^2 (\mu = \pi/a) = -0.993$ corresponding to a vanishing one-loop renormalized quark mass. We calculated the quasi-PDF with the Wilson-Clover action with bare quark mass ranging from $am = -4$ to $am = -0.05$ so that we can cover

² We also compared our bare quark mass am_0 at $c_{\text{sw}} = 0$, $r = 1$ with the numerical result in Ref. [37], we

$$\frac{2\pi}{\alpha_s C_F} \tilde{q}_{abc}^{\text{WC}} \left(x, a = 2^n \text{fm}, P_3 = \frac{3\pi}{2} \text{fm}^{-1}, m = \frac{\pi}{2} \text{fm}^{-1}, r = \frac{1}{2} \right)$$

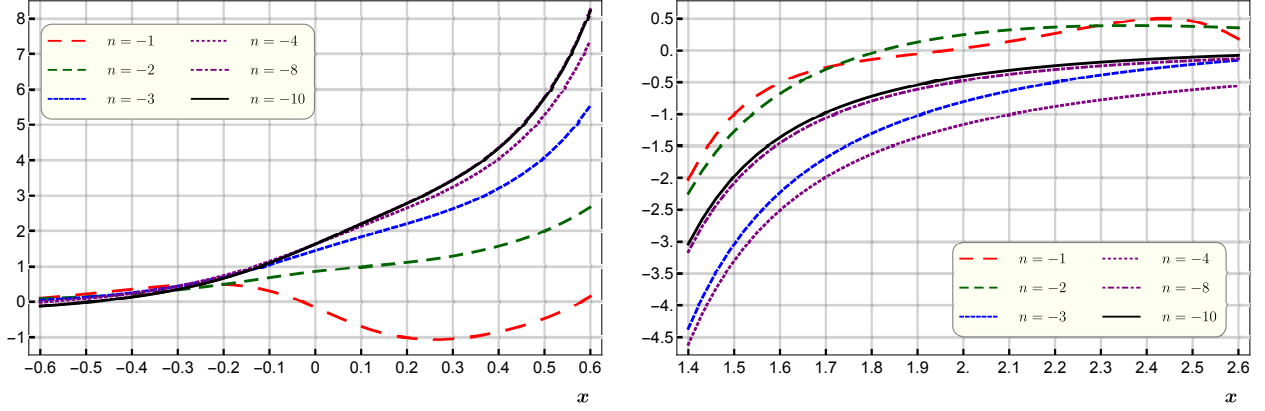


Figure 7: Numerical results for the quasi-PDF in Wilson-Clover lattice fermion action with non-zero bare quark mass and different lattice spacing.

the uncertainty from the strong coupling constant. The corresponding numerical results are shown in Fig. 9. The collinear divergence is still absent in the negative bare quark mass case.

The difference between the quasi-PDF calculated with the naïve fermion and the Wilson-Clover fermion action is

$$\delta\tilde{q}(x, P_3) = \tilde{q}^{\text{WC}}(x, P_3) - \tilde{q}^{\text{nv}}(x, P_3). \quad (47)$$

The corresponding numerical results are shown in Fig.10, we find that $\delta\tilde{q}(x, P_3)$ converges to a non-vanishing distribution under $a \rightarrow 0$ limit. Since $\lim_{a \rightarrow 0} \tilde{q}^{\text{nv}}(x, P_3) = q(x, P_3)$, $\tilde{q}^{\text{WC}}(x, P_3)$ can not recover the continuum quasi-PDF $q(x, P_3)$. $\delta\tilde{q}(x, P_3)$ comes from the Wilson term in the action and a simple series expansion shows that the k -integrand of $\delta\tilde{q}(x, P_3)$ is of the order of $\mathcal{O}(a^1)$ and thus can be viewed as $\mathcal{O}(a^1)$ corrections to the quasi-PDF calculated with the naïve fermion action ($\tilde{q}^{\text{nv}}(x, P_3)$). However, the UV region $k_\perp \sim \mathcal{O}(a^{-1})$ breaks the expansion and the k_\perp -integration turns out to be $\mathcal{O}(a^0)$ and therefore mixes with the quasi-PDF calculated with the naïve fermion action. This mixing is clearly visible in Fig. 10 where we see that in the $a \rightarrow 0$ limit, $\delta\tilde{q}(x, P_3)$ converges to a non-zero distribution. The mixing behavior is due to the fact that $\delta q(x, P_3)$ contains power

get

$$am_0 = -0.0158473C_F g_s^2 - 0.309866C_F g_s^2, \quad \text{Ref. [37],}$$

$$am_0 = -0.0158475C_F g_s^2 - 0.309865C_F g_s^2, \quad \text{this work, setting } c_{\text{SW}} = 0, r = 1,$$

where the first and second term correspond to the sunset and tadpole diagram, respectively. The relative difference is of the order of 10^{-6} .

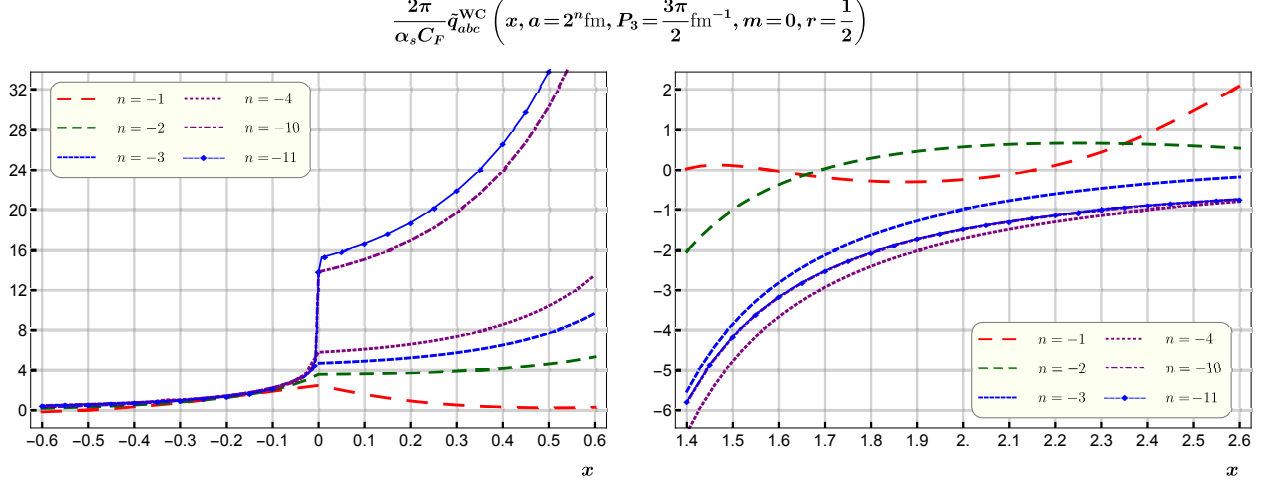


Figure 8: Numerical results for the quasi-PDF in Wilson-Clover lattice fermion action with vanishing bare quark mass and different lattice spacing. There is no collinear divergence in the numerical results.

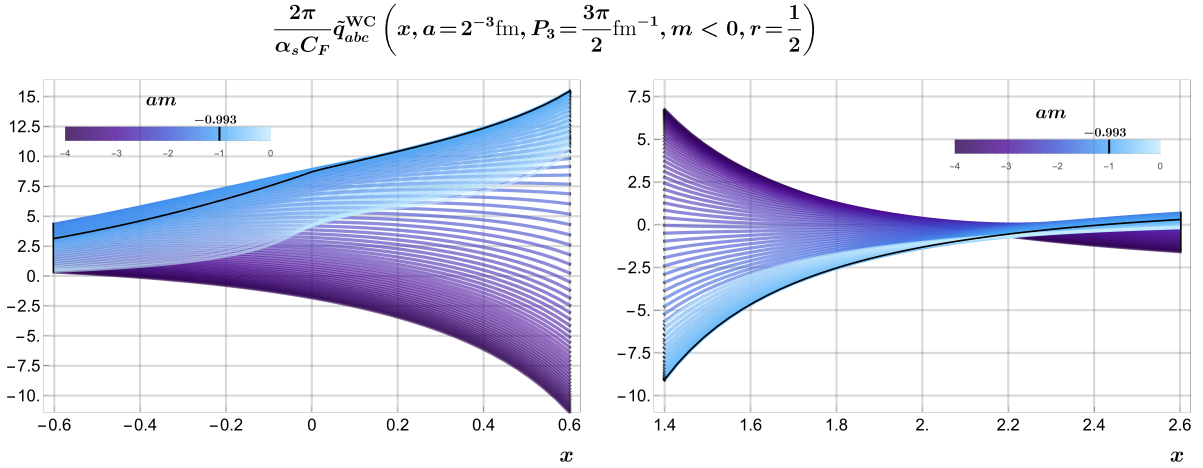


Figure 9: Numerical results for the quasi-PDF in Wilson-Clover lattice fermion action with negative bare quark masses $-4 \leq am \leq -0.05$, which is around the critical mass $am_0 = -0.993$ (black solid line). The collinear divergence is still absent in negative bare quark mass case.

divergent UV terms in the $a \rightarrow 0$ limit, e.g. after k_4 -integrated out

$$\delta \tilde{q}_{bc}^{\text{WC}}(x, P_3) \supset \int_{-\frac{\pi}{a}}^{\frac{\pi}{a}} \frac{d^2 \mathbf{k}_\perp}{8\pi^3} \frac{8g_s^2 C_F am r \Pi_-^2 \widehat{2k}_\perp^2 e^{iaP_4} \widehat{P} - \widehat{k}_3}{3a (\Pi_- - \Pi_+) \prod_{i=1}^4 (\Pi_- - z_i) \widehat{P} - \widehat{k}_3}. \quad (48)$$

In order to extract its UV behavior, we expand its continuum limit at $|\mathbf{k}_\perp| \rightarrow \infty$, which gives

$$\int \frac{d^2 \mathbf{k}_\perp}{16\pi^3} \frac{g_s^2 C_F m P_3}{P_0^2} \frac{a}{|\mathbf{k}_\perp|} + \dots \quad (49)$$

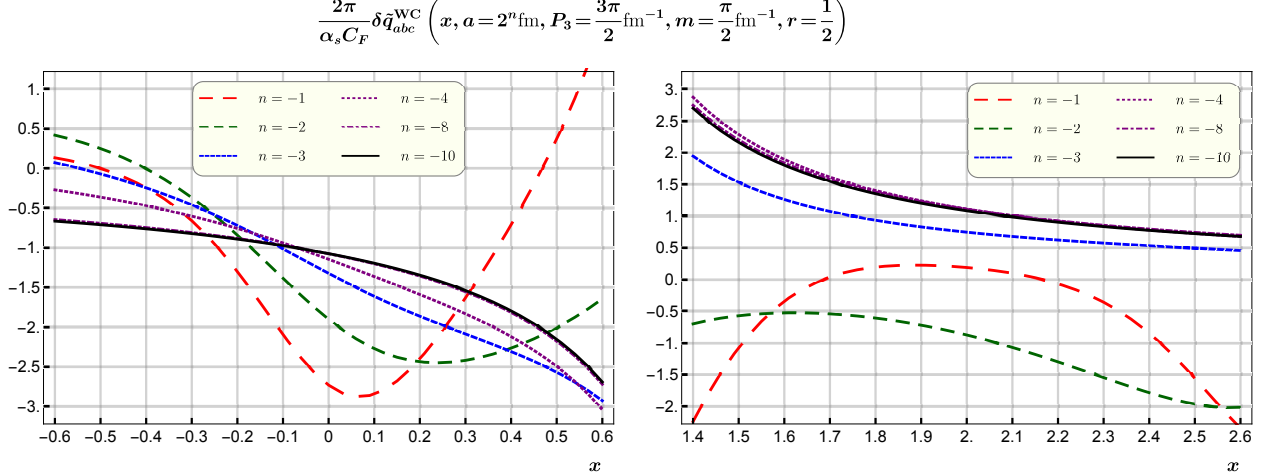


Figure 10: Numerical results of $\mathcal{O}(a^n)$ with $n \geq 1$ corrections $\delta \tilde{q}(x, a, P_3)$ to quasi-PDF in naïve lattice fermion action. The $\mathcal{O}(a^n)$ with $n \geq 1$ corrections do not vanish in the $a \rightarrow 0$ limit.

After integrating out \mathbf{k}_\perp , the power divergent UV integrand in the above equation gives a contribution proportional to a^{-1} which cancels the a^1 prefactor and therefore contributes to the integral at the order $\mathcal{O}(a^0)$. The mixing between higher and lower order in a already appears in the LPT calculation of the fermion self-energy with Wilson fermions [37]. The mixing indicates that some non-perturbative matching methods for quasi-PDF is required.

V. SUMMARY

The PDFs are one of the most essential non-perturbative quantities in QCD and they encode the dynamics of the QCD fundamental degrees of freedom: quarks and gluons inside a hadron. The PDFs can be measured by high energy scattering experiments and they are also widely used in experiments involving hadrons. The first principal determination of PDFs is still a very challenging area in QCD research. Large momentum effective field theory is developed to improve the first principal QCD calculation of the PDFs and its generalizations.

In this work, we calculated the quark-in-quark quasi-PDF $\tilde{q}(x, P_3)$ with naïve fermion action ($\tilde{q}^{\text{nv}}(x)$) and quasi-PDF with Wilson-Clover fermion action ($\tilde{q}^{\text{WC}}(x)$). We showed analytically that the \mathbf{k}_\perp -unintegrated $\tilde{q}^{\text{nv}}(x)$ exactly reduces to the continuum quasi-PDF in the zero lattice spacing limit. From the analytical \mathbf{k}_\perp -unintegrated $\tilde{q}^{\text{nv}}(x)$, we found that the collinear divergence is absent in the LPT calculated quasi-PDF at finite lattice spacing. We also compared the collinear behavior of $\tilde{q}^{\text{nv}}(x)$ and the continuum \mathbf{k}_\perp -integrated quasi-PDF numerically, and found that the limit of massless quark and zero lattice spacing do not commute. Our findings demonstrate that the proper limit to recover the collinear divergence of the continuum quasi-PDF should be $aP_3^2 \approx m$ and $m \ll P_3$, while the limit to fully recover the continuum quasi-PDF is $aP_3^2 \ll m \ll P_3$. These two conditions are based on perturbative calculations, therefore they should not be applied to non-perturbative lattice calculations which do not contain the collinear divergence because of the non-perturbative effects. The difference between $\tilde{q}^{\text{WC}}(x)$ and $\tilde{q}^{\text{nv}}(x)$ ($\delta \tilde{q}(x, P_3) = \tilde{q}^{\text{WC}}(x) - \tilde{q}^{\text{nv}}(x)$) can be

viewed as a $\mathcal{O}(a^1)$ correction to $\tilde{q}^{\text{nv}}(x)$ is due to the Wilson term and it contains UV power divergent integrands. These UV power divergent integrands render $\mathcal{O}(a^1)$ corrections that mix with $\tilde{q}^{\text{nv}}(x)$. This mixing indicates that a non-perturbative matching is required, and will be a subject of future research.

Acknowledgments

We thank Evan Berkowitz for useful discussions. X.X. also thanks Jian-Hui Zhang and Yong Zhao for discussions. We acknowledge financial support from the Deutsche Forschungsgemeinschaft (Sino-German CRC 110). The work of UGM was also supported by the Chinese Academy of Sciences (CAS) President's International Fellowship Initiative (PIFI) (Grant No.2017VMA0025).

Appendix A: Expressions For k_4 -Integration of quasi-PDF in naïve Lattice Fermion

The k_4 -integration of quasi-PDF calculated with naïve fermion action is given by the follows and in which $k_3 = xP_3$

$$\begin{aligned}
& \tilde{q}_a^{\text{nv}}(x) \\
&= P_3 g_s^2 C_F \int_{-\frac{\pi}{a}}^{\frac{\pi}{a}} \frac{d^2 \mathbf{k}_\perp}{(2\pi)^2} \left[\frac{a\sqrt{\Gamma_-} e^{iaP_4} \left(a^2 \left(-\widetilde{k} + \widetilde{P}_3^2 + \widetilde{\mathbf{k}}_\perp^2 \right) + 2 \right) + a^2 \Gamma_- e^{2iaP_4} + 1}{16\pi^3 a (\Gamma_- - \Gamma_+) (a\Pi_- - \sqrt{\Gamma_-}) (a\Pi_+ - \sqrt{\Gamma_-})} \right. \\
& \quad \left. + \left\langle \sqrt{\Gamma_-} \rightarrow -\sqrt{\Gamma_-} \right\rangle \right] + \frac{\Pi_- \left(a^4 \Pi_- e^{iaP_4} \left(-\widetilde{k} + \widetilde{P}_3^2 + \widetilde{\mathbf{k}}_\perp^2 \right) + (1 + a^2 \Pi_- e^{iaP_4})^2 \right)}{8\pi^3 a (\Pi_- - \Pi_+) (\Gamma_- - a^2 \Pi_-^2) (\Gamma_+ - a^2 \Pi_-^2)} \\
& \quad + \mathcal{F}_1(\mathcal{X}, \mathcal{Y}) + \frac{4m^2}{2\widehat{k}_3 \widehat{2P}_3} \mathcal{F}_1 \left(-a^2 \widetilde{k} + \widetilde{P}_3^2, a^2 \widetilde{\mathbf{k}}_\perp^2 - 10 \right) + \frac{i\widehat{2P}_4 (a^4 \Pi_-^2 - 1)}{a^3 \Pi_- \widehat{2k}_3 \widehat{2P}_3} \\
& \quad \times \mathcal{F}_1 \left(a^2 \widetilde{k} + \widetilde{P}_3^2, -a^2 \widetilde{\mathbf{k}}_\perp^2 + 6 \right) + \mathcal{F}_2 \left(\sqrt{\Gamma_-}, a^2 \widetilde{k} + \widetilde{P}_3^2 \right) + \frac{4m^2}{2\widehat{k}_3 \widehat{2P}_3} \mathcal{F}_2 \left(\sqrt{\Gamma_-}, -a^2 \widetilde{k} + \widetilde{P}_3^2 \right) \\
& \quad + \left\langle \mathcal{F}_2 \left(-\sqrt{\Gamma_-}, a^2 \widetilde{k} + \widetilde{P}_3^2 \right) + \frac{4m^2}{2\widehat{k}_3 \widehat{2P}_3} \mathcal{F}_2 \left(-\sqrt{\Gamma_-}, -a^2 \widetilde{k} + \widetilde{P}_3^2 \right) \right\rangle - \frac{a^2 \widetilde{k} + \widetilde{P}_3^2 + a^2 \widetilde{\mathbf{k}}_\perp^2 - 2}{16\pi^3 a^8 \Gamma_- (\Gamma_- - \Gamma_+) \widehat{3\widehat{2P}_3}} \\
& \quad \times \left[\frac{i\widehat{2k}_3 \widehat{2P}_4 e^{iaP_4} \left(-2a^4 \Gamma_-^2 + a^3 \sqrt{\Gamma_-} (\Pi_- + \Pi_+) (a^2 \Gamma_- - 1) + 2e^{2iaP_4} \right)}{(\sqrt{\Gamma_-} - a\Pi_-)^2 (\sqrt{\Gamma_-} - a\Pi_+)^2 (a^2 \Gamma_- - 1)^{-2}} + \left\langle \sqrt{\Gamma_-} \rightarrow -\sqrt{\Gamma_-} \right\rangle \right] \\
& \quad + \left\{ \frac{a^{-7} \Gamma_-^{-1} (\Gamma_- - \Gamma_+)^{-3} \widehat{2k}_3 \widehat{2P}_4}{16\pi^3 \widehat{2P}_3 (\sqrt{\Gamma_-} - a\Pi_-)^2 (\sqrt{\Gamma_-} - a\Pi_+)^2} \left[-i\sqrt{\Gamma_-} (a^2 \Gamma_- - 1)^2 \right. \right. \\
& \quad \times \left(2a^3 \sqrt{\Gamma_-} (\Pi_- + \Pi_+) (e^{2iaP_4} - 1) + 3a^2 \Gamma_- - (a^2 \Gamma_- + 3) e^{4iaP_4} + 1 \right) \\
& \quad \left. \left. - ia^4 \Gamma_-^{5/2} (a^2 \Gamma_- - 2) (a^2 \Gamma_- - 1) e^{2iaP_4} - i\sqrt{\Gamma_-} (2a^4 \Gamma_-^2 - a^2 (4\Gamma_- + \Gamma_+) + 3) e^{2iaP_4} \right] \right\} \\
& \quad + \left\langle \sqrt{\Gamma_-} \rightarrow -\sqrt{\Gamma_-} \right\rangle \left. \right\} + \left\{ \frac{a^{-7} \Gamma_-^{-1} (\Gamma_- - \Gamma_+)^{-3} \widehat{2k}_3 \left(\widehat{2k}_3 \widehat{2P}_3 + 4m^2 \right)}{16\pi^3 \widehat{2P}_3 (\sqrt{\Gamma_-} - a\Pi_-)^2 (\sqrt{\Gamma_-} - a\Pi_+)^2} \right\}
\end{aligned}$$

$$\begin{aligned}
& \times \left[-4a^6\Gamma_-^3 - 4a^2\Gamma_- e^{4iaP_4} + e^{2iaP_4} \left(a^5\Gamma_-^{3/2} (\Pi_- + \Pi_+) (a^4\Gamma_-^2 + 3) - 2(a^4\Gamma_-^2 + 1)^2 \right) \right. \\
& \left. + a^3\sqrt{\Gamma_-} (\Pi_- + \Pi_+) (3a^4\Gamma_-^2 + 1) \right] + \langle \sqrt{\Gamma_-} \rightarrow -\sqrt{\Gamma_-} \rangle \Big\} \\
& + \left\langle \frac{i\Gamma_- \widehat{2P}_4 (a^2\Gamma_- (a^2\Gamma_- - 3) + 2) - a(\Pi_- + \Pi_+) (a^4\Gamma_-^2 + 3) (\widehat{2k}_3 \widehat{2P}_3 + 4m^2)}{8\pi^3 a^3 (\Gamma_- - \Gamma_+)^3 \widehat{2P}_3 (a\Pi_- + \sqrt{\Gamma_-})^2 (a\Pi_+ + \sqrt{\Gamma_-})^2 \Gamma_-^{-\frac{1}{2}} \widehat{2k}_3^{-1} e^{-2iaP_4}} \right\rangle, \quad (\text{A1})
\end{aligned}$$

where $\langle \sqrt{\Gamma_-} \rightarrow -\sqrt{\Gamma_-} \rangle$ means performing the replacement to the previous term within the same $\{\dots\}$ or $[\dots]$. The functions $\mathcal{F}_{1,2}$ are defined as

$$\mathcal{F}_1(\mathcal{X}, \mathcal{Y}) = \frac{a\Pi_-^3 \widehat{2k}_3^2 (-a^2\Pi_- e^{iaP_4} (\mathcal{X} + \mathcal{Y}) + a^4\Pi_-^2 e^{2iaP_4} + 1)}{4\pi^3 (\Pi_- - \Pi_+) (\Gamma_- - a^2\Pi_-^2)^2 (\Gamma_+ - a^2\Pi_-^2)^2} \quad (\text{A2a})$$

$$\mathcal{F}_2(\mathcal{X}, \mathcal{Y}) = \frac{-\widehat{2k}_3^2 e^{iaP_4} (3a^6\Gamma_-^3 + (a^4\Gamma_-^2 + 3) e^{2iaP_4} + a^2\Gamma_- - 2a^3\mathcal{X} (\Pi_- + \Pi_+) (a^4\Gamma_-^2 + 1))}{16\pi^3 a^6 \mathcal{X} (\Gamma_- - \Gamma_+)^3 (\mathcal{X} - a\Pi_-)^2 (\mathcal{X} - a\Pi_+)^2 (a^2\widetilde{\mathbf{k}}_\perp^2 + 2 - \mathcal{Y})^{-1}} \quad (\text{A2b})$$

The terms inside $\langle \rangle$ are the contributions from the unphysical quark pole z_q^- and they are of order $\mathcal{O}(a^2)$.

It is straight forward to verify that diagram *b* and *c* give an identical contribution, which reads

$$\begin{aligned}
\tilde{q}_{b/c}^{\text{nv}}(x) = & \int_{-\frac{\pi}{a}}^{\frac{\pi}{a}} d^2\mathbf{k}_\perp \frac{g_s^2 C_F}{16\pi^3} \frac{P_3 e^{iaP_4} \widetilde{k + P_3}}{a \widehat{2P}_3 \widetilde{k - P_3}} \left\{ \frac{2\Pi_- (a^3\Pi_- (\widehat{2k}_3 \widehat{2P}_3 - 4m^2) + i\widehat{2P}_4 (a^4\Pi_-^2 - 1))}{-(\Pi_- - \Pi_+) (a^2\Pi_-^2 - \Gamma_-) (a^2\Pi_-^2 - \Gamma_+)} \right. \\
& \left. + \left[\frac{a^2\sqrt{\Gamma_-} (\widehat{2k}_3 \widehat{2P}_3 - 4m^2) + i\widehat{2P}_4 (1 - a^2\Gamma_-)}{(\Gamma_- - \Gamma_+) (a\Pi_- + \sqrt{\Gamma_-}) (a\Pi_+ + \sqrt{\Gamma_-})} + \langle \sqrt{\Gamma_-} \rightarrow -\sqrt{\Gamma_-} \rangle \right] \right\}. \quad (\text{A3})
\end{aligned}$$

The k_4 Integration of diagram *d* gives

$$\tilde{q}_d(x) = \frac{g_s^2 C_F}{8\pi^3} \int_{-\frac{\pi}{a}}^{\frac{\pi}{a}} d^2\mathbf{k}_\perp \frac{P_3 e^{iaP_4}}{a(\Pi_- - \Pi_+) \widetilde{P - k_3}}. \quad (\text{A4})$$

We also have checked that the $a \rightarrow 0$ limit of above the \mathbf{k}_\perp -integrands coincide with the \mathbf{k}_\perp unintegrated quasi-PDF calculated directly in the continuum.

-
- [1] X. D. Ji, Phys. Rev. Lett. **78**, 610 (1997) doi:10.1103/PhysRevLett.78.610 [hep-ph/9603249].
[2] X. Ji, X. Xiong and F. Yuan, Phys. Rev. Lett. **109**, 152005 (2012) doi:10.1103/PhysRevLett.109.152005 [arXiv:1202.2843 [hep-ph]].

- [3] Y. B. Yang, R. S. Sufian, A. Alexandru, T. Draper, M. J. Glatzmaier, K. F. Liu and Y. Zhao, Phys. Rev. Lett. **118**, no. 10, 102001 (2017) doi:10.1103/PhysRevLett.118.102001 [arXiv:1609.05937 [hep-ph]].
- [4] J. C. Peng, W. C. Chang, H. Y. Cheng, T. J. Hou, K. F. Liu and J. W. Qiu, Phys. Lett. B **736**, 411 (2014) doi:10.1016/j.physletb.2014.07.050 [arXiv:1401.1705 [hep-ph]].
- [5] W. C. Chang and J. C. Peng, Prog. Part. Nucl. Phys. **79**, 95 (2014) doi:10.1016/j.pnpnp.2014.08.002 [arXiv:1406.1260 [hep-ph]].
- [6] J. C. Collins, D. E. Soper and G. F. Sterman, Adv. Ser. Direct. High Energy Phys. **5**, 1 (1989) doi:10.1142/9789814503266_0001 [hep-ph/0409313].
- [7] A. D. Martin, W. J. Stirling, R. S. Thorne and G. Watt, Eur. Phys. J. C **63**, 189 (2009) doi:10.1140/epjc/s10052-009-1072-5 [arXiv:0901.0002 [hep-ph]].
- [8] H. L. Lai, M. Guzzi, J. Huston, Z. Li, P. M. Nadolsky, J. Pumplin and C.-P. Yuan, Phys. Rev. D **82**, 074024 (2010) doi:10.1103/PhysRevD.82.074024 [arXiv:1007.2241 [hep-ph]].
- [9] S. Dulat *et al.*, Phys. Rev. D **93**, no. 3, 033006 (2016) doi:10.1103/PhysRevD.93.033006 [arXiv:1506.07443 [hep-ph]].
- [10] R. Gauld and J. Rojo, Phys. Rev. Lett. **118**, no. 7, 072001 (2017) doi:10.1103/PhysRevLett.118.072001 [arXiv:1610.09373 [hep-ph]].
- [11] J. C. Collins and D. E. Soper, Nucl. Phys. B **194**, 445 (1982). doi:10.1016/0550-3213(82)90021-9
- [12] X. Ji, Phys. Rev. Lett. **110**, 262002 (2013) doi:10.1103/PhysRevLett.110.262002 [arXiv:1305.1539 [hep-ph]].
- [13] X. Ji, Sci. China Phys. Mech. Astron. **57**, 1407 (2014) doi:10.1007/s11433-014-5492-3 [arXiv:1404.6680 [hep-ph]].
- [14] X. Xiong, X. Ji, J. H. Zhang and Y. Zhao, Phys. Rev. D **90**, no. 1, 014051 (2014) doi:10.1103/PhysRevD.90.014051 [arXiv:1310.7471 [hep-ph]].
- [15] Y. Q. Ma and J. W. Qiu, arXiv:1404.6860 [hep-ph].
- [16] Y. Q. Ma and J. W. Qiu, Int. J. Mod. Phys. Conf. Ser. **37**, 1560041 (2015) doi:10.1142/S2010194515600411 [arXiv:1412.2688 [hep-ph]].
- [17] J. W. Chen, S. D. Cohen, X. Ji, H. W. Lin and J. H. Zhang, Nucl. Phys. B **911**, 246 (2016) doi:10.1016/j.nuclphysb.2016.07.033 [arXiv:1603.06664 [hep-ph]].
- [18] X. Ji and J. H. Zhang, Phys. Rev. D **92**, 034006 (2015) doi:10.1103/PhysRevD.92.034006 [arXiv:1505.07699 [hep-ph]].
- [19] T. Ishikawa, Y. Q. Ma, J. W. Qiu and S. Yoshida, arXiv:1609.02018 [hep-lat].
- [20] J. W. Chen, X. Ji and J. H. Zhang, Nucl. Phys. B **915**, 1 (2017) doi:10.1016/j.nuclphysb.2016.12.004 [arXiv:1609.08102 [hep-ph]].
- [21] H. n. Li, Phys. Rev. D **94**, no. 7, 074036 (2016) doi:10.1103/PhysRevD.94.074036 [arXiv:1602.07575 [hep-ph]].
- [22] X. Ji, A. Schäfer, X. Xiong and J. H. Zhang, Phys. Rev. D **92**, 014039 (2015) doi:10.1103/PhysRevD.92.014039 [arXiv:1506.00248 [hep-ph]].
- [23] X. Xiong and J. H. Zhang, Phys. Rev. D **92**, no. 5, 054037 (2015) doi:10.1103/PhysRevD.92.054037 [arXiv:1509.08016 [hep-ph]].
- [24] H. W. Lin, J. W. Chen, S. D. Cohen and X. Ji, Phys. Rev. D **91**, 054510 (2015) doi:10.1103/PhysRevD.91.054510 [arXiv:1402.1462 [hep-ph]].
- [25] C. Alexandrou, K. Cichy, V. Drach, E. Garcia-Ramos, K. Hadjiyiannakou, K. Jansen, F. Steffens and C. Wiese, Phys. Rev. D **92**, 014502 (2015) doi:10.1103/PhysRevD.92.014502 [arXiv:1504.07455 [hep-lat]].

- [26] C. E. Carlson and M. Freid, arXiv:1702.05775 [hep-ph].
- [27] R. A. Briceño, M. T. Hansen and C. J. Monahan, arXiv:1703.06072 [hep-lat].
- [28] M. Constantinou and H. Panagopoulos, arXiv:1705.11193 [hep-lat].
- [29] C. Alexandrou, K. Cichy, M. Constantinou, K. Hadjiyiannakou, K. Jansen, H. Panagopoulos and F. Steffens, arXiv:1706.00265 [hep-lat].
- [30] J. W. Chen, T. Ishikawa, L. Jin, H. W. Lin, Y. B. Yang, J. H. Zhang and Y. Zhao, arXiv:1706.01295 [hep-lat].
- [31] R. Horsley, H. Perlt, P. E. L. Rakow, G. Schierholz and A. Schiller, Phys. Rev. D **78**, 054504 (2008) doi:10.1103/PhysRevD.78.054504 [arXiv:0807.0345 [hep-lat]].
- [32] P. Weisz, Nucl. Phys. B **212**, 1 (1983). doi:10.1016/0550-3213(83)90595-3
- [33] P. Weisz and R. Wohlert, Nucl. Phys. B **236**, 397 (1984) Erratum: [Nucl. Phys. B **247**, 544 (1984)]. doi:10.1016/0550-3213(84)90563-7, 10.1016/0550-3213(84)90543-1
- [34] E. H. Muller *et al.*, PoS LAT **2009**, 241 (2009) [arXiv:0909.5126 [hep-lat]].
- [35] Christopher John Monahan, *The application of automated perturbation theory to lattice QCD*. PhD thesis, University of Cambridge, 2011.
- [36] X. Ji, J. H. Zhang and Y. Zhao, arXiv:1706.07416 [hep-ph].
- [37] S. Capitani, Phys. Rept. **382**, 113 (2003) doi:10.1016/S0370-1573(03)00211-4 [hep-lat/0211036].